

DTIC FILE COPY

2

AD-A212 271

# NAVAL POSTGRADUATE SCHOOL

## Monterey, California



# THESIS

DTIC  
ELECTE  
SEP 12 1989  
S E D

AN APPROACH TO LOW TEMPERATURE  
HIGH STRAIN RATE SUPERPLASTICITY  
IN ALUMINUM ALLOY 2090

by

Michael Wayne Reedy

June 1989

Thesis Advisor:

Terry McNelley

Approved for public release; distribution is unlimited.

89 9 12 015

Unclassified

security classification of this page

## REPORT DOCUMENTATION PAGE

1a Report Security Classification <b>Unclassified</b>			1b Restrictive Markings		
2a Security Classification Authority			3 Distribution/Availability of Report		
2b Declassification Downgrading Schedule			Approved for public release; distribution is unlimited.		
4 Performing Organization Report Number(s)			5 Monitoring Organization Report Number(s)		
6a Name of Performing Organization Naval Postgraduate School		6b Office Symbol (if applicable)	7a Name of Monitoring Organization Naval Postgraduate School		
6c Address (city, state, and ZIP code) Monterey, CA 93943-5000			7b Address (city, state, and ZIP code) Monterey, CA 93943-5000		
8a Name of Funding Sponsoring Organization		8b Office Symbol (if applicable)	9 Procurement Instrument Identification Number		
8c Address (city, state, and ZIP code)			10 Source of Funding Numbers		
			Program Element No	Project No	Task No
			Work Unit Accession No		
11 Title (include security classification) <b>AN APPROACH TO LOW TEMPERATURE HIGH STRAIN RATE SUPERPLASTICITY IN ALUMINUM ALLOY 2090</b>					
12 Personal Author(s) <b>Michael Wayne Reedy</b>					
13a Type of Report Master's Thesis		13b Time Covered From To		14 Date of Report (year, month, day) June 1989	
				15 Page Count 80	
16 Supplementary Notation The views expressed in this thesis are those of the author and do not reflect the official policy or position of the Department of Defense or the U.S. Government.					
17 Cosati Codes			18 Subject Terms (continue on reverse if necessary and identify by block number)		
Field	Group	Subgroup	superplasticity, Al2090,.		
19 Abstract (continue on reverse if necessary and identify by block number)					
Successful study of processing, microstructural development and superplasticity in Al-Mg alloys has been extended to the Lithium-containing 2090 alloy. Attainment of superior superplastic response in the 2090 alloy has proven more difficult. Successive reductions in the temperature at which rolling was conducted have resulted in moderate improvement to superplastic response. Modification to the rolling schedule has resulted in a continuously increasing strain rate during rolling while recovery temperature and rolling speed are unaltered from previous work. <i>Superplasticity. (JES)</i>					
20 Distribution Availability of Abstract <input checked="" type="checkbox"/> unclassified unlimited <input type="checkbox"/> same as report <input type="checkbox"/> DTIC users			21 Abstract Security Classification <b>Unclassified</b>		
22a Name of Responsible Individual T.R. McNelley			22b Telephone (include Area code) (408) 646-2589		22c Office Symbol 69Mc

DD FORM 1473, 84 MAR

83 APR edition may be used until exhausted  
All other editions are obsolete

security classification of this page

Unclassified

Approved for public release; distribution is unlimited.

An Approach to Low Temperature  
High Strain Rate Superplasticity  
in Aluminum Alloy 2090

by

Michael Wayne Reedy  
Lieutenant, United States Navy  
B.S., United States Naval Academy, 1979

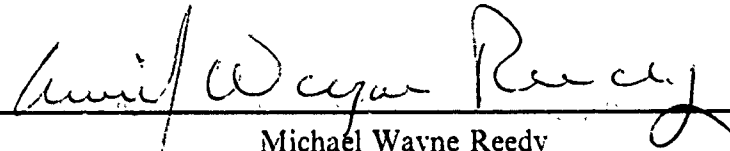
Submitted in partial fulfillment of the  
requirements for the degree of

MASTER OF SCIENCE IN MECHANICAL ENGINEERING

from the

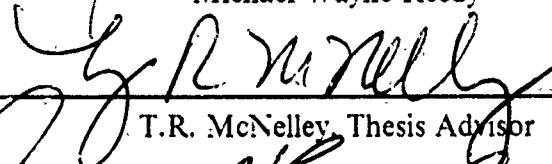
NAVAL POSTGRADUATE SCHOOL  
June 1989

Author:

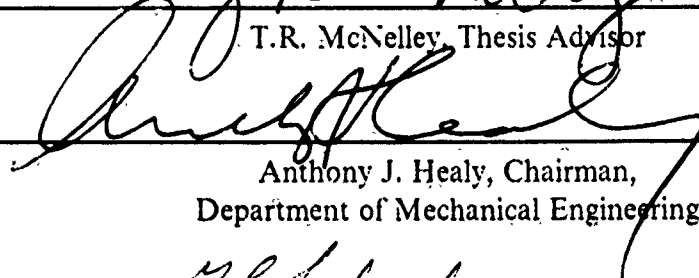


Michael Wayne Reedy

Approved by:



T.R. McNelley, Thesis Advisor



Anthony J. Healy, Chairman,  
Department of Mechanical Engineering



Gordon E. Schacher,  
Dean of Science and Engineering

## **ABSTRACT**

Successful study of processing, microstructural development and superplasticity in Al-Mg alloys has been extended to the Lithium-containing 2090 alloy. Attainment of superior superplastic response in the 2090 alloy has proven more difficult. Successive reductions in the temperature at which rolling was conducted have resulted in moderate improvement to superplastic response. Modification to the rolling schedule has resulted in a continuously increasing strain rate during rolling while recovery temperature and rolling speed are unaltered from previous work.

## TABLE OF CONTENTS

I.	INTRODUCTION . . . . .	1
A.	ALUMINUM ALLOY 2090 . . . . .	1
B.	SUPERPLASTICITY . . . . .	3
C.	REQUIREMENTS FOR SUPERPLASTICITY . . . . .	4
II.	BACKGROUND . . . . .	6
A.	DEVELOPMENT OF LOW TEMPERATURE SUPERPLASTIC Al-Mg ALLOY . . . . .	6
B.	THE STRAIN RATE SENSITIVITY COEFFICIENT . . . . .	9
C.	APPLICATION OF TMP TO THE Al-2090 ALLOY . . . . .	10
III.	EXPERIMENTAL PROCEDURE . . . . .	14
A.	MATERIAL . . . . .	14
B.	PROCESSING . . . . .	14
1.	Plate Sectioning and Billet Preparation . . . . .	14
2.	Solution Treatment and Forging . . . . .	15
3.	Rolling . . . . .	15
4.	Sample Preparation . . . . .	18
C.	TESTING . . . . .	21
D.	METALLOGRAPHY . . . . .	22

IV. RESULTS AND DISCUSSION . . . . .	23
A. MICROSTRUCTURAL CONDITION PRIOR TO ROLLING . . . . .	23
B. MICROSTRUCTURAL CONDITION AFTER ROLLING . . . . .	24
C. RESULTS OF MECHANICAL TESTING . . . . .	28
D. CONDITION OF MICROSTRUCTURE AFTER DEFORMATION . . . . .	40
E. EVALUATION OF STRAIN RATE COEFFICIENTS . . . . .	44
F. SUMMARY . . . . .	47
V. CONCLUSIONS . . . . .	48
VI. RECOMMENDATIONS . . . . .	49
APPENDIX A . . . . .	50
APPENDIX B . . . . .	52

## LIST OF FIGURES

	PAGE
<b>Figure 1.</b> Plot of Warm Rolling Strain Rate vs. Rolling Pass: Depicting the Increased Warm Rolling Strain Rate used during the Final Pass of this Study over that used in Previous Work. . . . .	19
<b>Figure 2.</b> Tensile Test Sample Dimensions. The Effective Gage Length is 0.5 Inches in All Cases while the Thickness is a Function of Final Rolling Strain. . . . .	20
<b>Figure 3.</b> Surface Micrograph of Material Rolled at 150 C for Final Five Passes. Scattered Inclusion Content Discernable. View is Representative (at optical level) of Surface Condition for each Rolling Scheme Covered in this Study.	25
<b>Figures 4 (a) and (b).</b> Long Transverse Optical Micrographs of Material Rolled at 150 C in Final Five Passes. Figure 4 (a) is Low in Inclusion Content, While 4 (b) Contains a Considerable Number of Inclusions Visible in the Banding. . . . . .	26
<b>Figures 5 (a) and (b).</b> Short Transverse Optical Micrographs of Material Rolled at 150 C in Final Five Passed. Figure 5 (a) is Low in Inclusion Content While 5 (b) Contains a Considerable Number of Inclusions Visible in the Banding.	27
<b>Figure 6.</b> Ductility vs. Tensile Test Temperature for Material Rolled at 300 C. . . . .	30
<b>Figure 7.</b> Ductility vs. Tensile Test Temperature for Material Rolled at 250 C in the Final Five Rolling Passes. . . . .	31
<b>Figure 8.</b> Ductility vs. Tensile Test Temperature for Material Rolled at 150 C in the Final Five Rolling Passes. . . . .	32
<b>Figure 9.</b> Flow Stress at True Strain of 10% vs. Test Temperature for Material Rolled at 300 C. . . . .	35

	PAGE
<b>Figure 10.</b> Flow Stress at True Strain of 10% vs. Test Temperature for Material Rolled at 250 C for the Final Five Rolling Passes. . . . .	36
<b>Figure 11.</b> Flow Stress at True Strain of 10% vs. Test Temperature for Material Rolled at 150 C for the Final Five Rolling Passes. . . . .	37
<b>Figure 12.</b> Historical Overview of Results of Testing at a Strain Rate of $6.67 \times 10^{-3} \text{ s}^{-1}$ , Depicting a General Trend Toward Improved Elongation as a Result of Refinements to Thermomechanical Processing (TMP). . . . .	38
<b>Figure 13.</b> Historical Overview of Results of Testing at a Strain Rate of $6.67 \times 10^{-4} \text{ s}^{-1}$ , Depicting a General Trend Toward Improved Elongation as a Result of Refinement to Thermomechanical Processing (TMP). . . . .	39
<b>Figure 14.</b> Long-Transverse Grip Section Micrograph of the Specimen Rolled at 150 C and Tested at 400 C and Strain Rate of $6.67 \times 10^{-3} \text{ s}^{-1}$ , Exhibiting an Extremely Fine Distribution of Second Phase Particles in a Matrix. . . .	41
<b>Figure 15.</b> Micrograph of the Long-Transverse Gage Section Shown in Comparison to Figure 14, Exhibiting Retention of the Fine Dispersion of the Second Phase, and only Slight Cavitation. . . . .	42
<b>Figure 16.</b> Micrograph of the Fracture Tip of the Specimen attaining 375% Elongation, Illustrating Limited Cavitation in the Unnecked Section, and Increasing Cavitation and Coarsening in the Vicinity of the Fracture Tip. . . . .	43
<b>Figure 17.</b> View of the Grip Section, Rolled at 150 C and Tested at 370 C and a Strain Rate of $6.67 \times 10^{-4} \text{ s}^{-1}$ , Depicting Similar Microstructure to the Grip Section in Figure 14 with the Exception of Greater Inclusion Content. . . . .	45



<b>Figure 18.</b> Corresponding Gage Section Micrograph to Figure 17, Depicting Retention of Fine Grain Structure, and an Inclusion Content Greater than that Shown in Figures 14 and 15, Possibly Contributing to Failure at an Elongation of only 308%. . . . .	46
---	----

## LIST OF FIGURES IN APPENDIXES

	PAGE
<b>Figure A-1.</b> Summary of Ductility Data . . . . .	50
<b>Figure A-2.</b> Historical Summary of Strain Rate Sensitivity Coefficients. . . . .	51
<b>Figure B-1.</b> True Stress vs. True Strain for Various Temperatures as Shown in the Legend. The Material was Rolled at a Temperature of 300 C, and Tested at a Strain Rate of $6.67 \times 10^{-2} \text{ s}^{-1}$ . . . . .	52
<b>Figure B-2.</b> True Stress vs. True Strain for Various Temperatures as Shown in the Legend. The Material was Rolled at a Temperature of 300 C, and Tested at a Strain Rate of $6.67 \times 10^{-3} \text{ s}^{-1}$ . . . . .	53
<b>Figure B-3.</b> True Stress vs. True Strain for Various Temperatures as Shown in the Legend. The Material was Rolled at a Temperature of 300 C, and Tested at a Strain Rate of $6.67 \times 10^{-4} \text{ s}^{-1}$ . . . . .	54
<b>Figure B-4.</b> True Stress vs. True Strain for Various Temperatures as Shown in the Legend. The Material was Rolled at a Temperature of 300 C, and Tested at a Strain Rate of $6.67 \times 10^{-5} \text{ s}^{-1}$ . . . . .	55
<b>Figure B-5.</b> True Stress vs. True Strain for Various Temperatures as Shown in the Legend. The Material was Rolled at a Temperature of 250 C for the Final Five Passes, and Tested at a Strain Rate of $6.67 \times 10^{-2} \text{ s}^{-1}$ . . . . .	56
<b>Figure B-6.</b> True Stress vs. True Strain for Various Temperatures as Shown in the Legend. The Material was Rolled at a Temperature of 250 C for the Final Five Passes, and Tested at a Strain Rate of $6.67 \times 10^{-3} \text{ s}^{-1}$ . . . . .	57
<b>Figure B-7.</b> True Stress vs. True Strain for Various Temperatures as Shown in the Legend. The Material was Rolled at a Temperature of 250 C for the Final Five Passes, and Tested at a Strain Rate of $6.67 \times 10^{-4} \text{ s}^{-1}$ . . . . .	58

- Figure B-8.** True Stress vs. True Strain for Various Temperatures as Shown in the Legend. The Material was Rolled at a Temperature of 250 C for the Final Five Passes, and Tested at a Strain Rate of  $6.67 \times 10^{-3} \text{ s}^{-1}$ . . . . . 59
- Figure B-9.** True Stress vs. True Strain for Various Temperatures as Shown in the Legend. The Material was Rolled at a Temperature of 150 C for the Final Five Passes, and Tested at a Strain Rate of  $6.67 \times 10^{-2} \text{ s}^{-1}$ . . . . . 60
- Figure B-10.** True Stress vs. True Strain for Various Temperatures as Shown in the Legend. The Material was Rolled at a Temperature of 150 C for the Final Five Passes, and Tested at a Strain Rate of  $6.67 \times 10^{-3} \text{ s}^{-1}$ . . . . . 61
- Figure B-11.** True Stress vs. True Strain for Various Temperatures as Shown in the Legend. The Material was Rolled at a Temperature of 150 C for the Final Five Passes, and Tested at a Strain Rate of  $6.67 \times 10^{-4} \text{ s}^{-1}$ . . . . . 62
- Figure B-12.** True Stress vs. True Strain for Various Temperatures as Shown in the Legend. The Material was Rolled at a Temperature of 150 C for the Final Five Passes, and Tested at a Strain Rate of  $6.67 \times 10^{-5} \text{ s}^{-1}$ . . . . . 63
- Figure B-13.** Log Stress vs. Log Strain Rate at a True Strain of 10%, for Various Test Temperatures as Listed in the Legend. For Material Rolled at 300 C. . . . . 64
- Figure B-14.** Log Stress vs. Log Strain Rate at a True Strain of 10%, for Various Test Temperatures as Listed in the Legend. For Material Rolled at 250 C in the Final Five Passes. . . . . 65
- Figure B-15.** Log Stress vs. Log Strain Rate at a True Strain of 10%, for Various Test Temperatures as Listed in the Legend. For Material Rolled at 150 C in the Final Five Passes. . . . . 66

## I. INTRODUCTION

Considerable study of superplasticity in Aluminum alloys has been conducted at the Naval Postgraduate School (NPS) in recent years. A series of experiments conducted on Aluminum-Magnesium alloys has resulted in the development of a successful thermomechanical process (TMP) leading to tensile test elongations up to 700% in Al-Mg alloys [Ref. 1] and in excess of 1000% in Al-Mg-Li alloy [Ref. 2]. These results generally are obtained at 300 C, a relatively low temperature reflecting extremely fine grain size achieved during TMP. Attempts to apply this successful TMP to the Aluminum-containing alloy 2090 have, to date, not been as successful.

### A. ALUMINUM ALLOY 2090

The alloy designated 2090 (containing Al-2.56 Wt% Cu-2.03 Wt% Li-0.12 Wt% Zr) has been developed by Alcoa as a high strength alloy at ambient temperatures. It is also seven to eight percent less dense and has an elastic modulus approximately ten percent higher than that of 7075 Aluminum, the alloy it was designed to replace [Ref. 3 & 4].

The 2090 alloy has attracted attention because Lithium is one of only two elements which when alloyed with Aluminum increases the elastic modulus and decreases the alloy density. The alternative is

Beryllium, an element with significant occupational health concerns associated with its practical use. Lithium is thus the element of choice to provide improvement in specific modulus and specific strength of Al alloys. These improvements naturally lead to weight savings, a very attractive asset in the aerospace field.

Others have reported extensive elongations, in 2090 suitably processed material. For example, Alcoa has reported elongations of 683-838% at 527 C and a strain rate of  $4.0 \times 10^{-4} \text{ s}^{-1}$  [Ref. 5], and 500-800% at 520 C and strain rates of  $2.0 \times 10^{-3} \text{ s}^{-1}$  and  $2.0 \times 10^{-4} \text{ s}^{-1}$  [Ref. 6]. While these results are impressive, cavitation during deformation at such a temperature is a recognized problem which leads to difficulties in maintaining minimum acceptable material properties. It is believed that strength and fracture toughness can be preserved in the material even after it has been superplastically formed by limiting the superplastic forming temperature to minimize cavitation. This may facilitate retention of fine grain structure in the alloy.

The focus of the research being conducted on the 2090 alloy at NPS is therefore to develop a TMP which results in extensive tensile elongations at relatively lower elevated temperature, and at strain rates comparable to those achieved in previous research on Aluminum-Magnesium alloys.

## B. SUPERPLASTICITY

Superplasticity refers to the ability of a material to attain large tensile elongation prior to suffering localized necking and fracture [Ref. 4]. Ideal superplastic materials should exhibit the following characteristics: [Ref. 7]

- adequate superplastic strain capability with reasonably isotropic superplastic properties
- low flow stress
- low susceptibility to cavitation during forming
- forming at temperatures within the solution treatment ranges
- low quench sensitivity
- good service properties after subsequent treatment

If 2090 can be made superplastic and to conform with the characteristics outlined above, a very valuable material will be available to the aerospace industry [Ref. 8]. The primary use of superplastic forming today is within the aerospace industry. For example superplastically formed frame nacelles have been produced for the B-1 aircraft [Ref. 9]. This was accomplished utilizing the Ti-6Al-4V alloy and demonstrates the versatility of superplastically formed materials and the importance of developing a processing technique for other alloys including the Al-2090 alloy.

### C. REQUIREMENTS FOR SUPERPLASTICITY

A series of experiments has been conducted at NPS in effort to apply the techniques successfully employed in the Al-Mg alloys. In this earlier work a TMP was developed to promote microstructural changes in the Al-Mg alloy by the continuous recrystallization (CRX) mechanism. This refers to recrystallization during the warm rolling portion of the TMP as in [Ref. 10] as well as during subsequent heating and superplastic deformation. This process also utilizes the precipitation of intermetallic phases to stabilize evolving grain structures. The phase  $T_2$  is believed to be the intermetallic phase which may be used to stabilize such structures and promote superplasticity in 2090 [Ref. 10].

Specific requirements for successful superplastic forming include the following [Ref. 11]:

- fine grain size: Typically, grain size less than 20  $\mu\text{m}$  is required.
- strength of the second phase: The relative strength of the matrix and second phase during superplastic flow is a parameter in the control of cavitation and therefore the elongation to failure.
- size and distribution of second phase: A second phase should be uniformly well distributed in the matrix. A fine, hard second phase particle can help inhibit

cavitation during superplastic forming.

-nature of grain boundary structures: Grain boundaries between adjacent matrix grains should be of a high-angle nature because grain boundary sliding (GBS) is the predominant mode of deformation during superplastic flow.

-mobility of grain boundaries: During grain boundary sliding high stresses develop at triple points and obstructions (second phase particles); grain boundary mobility permits relief of these stresses.

-grain shape: Grains should be equiaxed in order that shear stresses developed allow grain boundary sliding to occur.

This current research extends previous work to achieve in 2090 the microstructural prerequisites outlined above by means of a TMP intended to promote recrystallization by a continuous reaction during processing.



## **II. BACKGROUND**

To appreciate the work conducted to date on the 2090 alloy the effort to understand the influence of process variables in the Al-Mg alloy work is first reviewed. This includes a brief discussion of the model which has been proposed to explain the process of continuous recrystallization during TMP. A review of the importance of strain rate sensitivity follows. Finally the lessons of the successful Al-Mg TMP development and the accompanying theory are applied to the work on 2090.

### **A. DEVELOPMENT OF LOW TEMPERATURE SUPERPLASTIC Al-Mg ALLOY**

In order to develop superplasticity in Aluminum alloys the effect of each phase of the thermomechanical process must be well understood. At NPS successful work in this area is represented by that completed with the Al-Mg and Al-Mg-X series alloys. Variables in the TMP include: the solution treatment and hot working parameters, including time and temperature variables; the schedule of reductions; total strain introduced into the material by the rolling schedule; the rolling temperature and the recovery time interval. Adjustment of

these several parameters eventually lead to success in the Al-Mg series, but not before considerable effort was expended.

In the deformation process the heavy straining of the material results in an increased dislocation density. At a sufficient temperature, recovery processes allow these dislocation to form sub-boundaries within grains. The essential feature of the proposed model in that the boundaries are stabilized by precipitated intermetallic particles, such that the boundaries may continue to absorb dislocations during anneals between subsequent rolling passes. By this means the boundaries will increase in misorientation and with sufficient cycles of straining and annealing be able to satisfy the requirement for high angle boundaries.

By increasing the reduction taken on the material per rolling pass the dislocation density produced would be increased. With increased dislocation density and with sufficient annealing time, the resultant enhancement of the formation of sub-boundaries and increase in grain boundary misorientation can be expected. A resultant increase in superplastic performance was shown to follow [Ref. 1].

The work of Hales, et al. [Ref. 12] demonstrated that Al -Mg alloys can be processed to exhibit boundary structures characterized by misorientations of 2-7 degrees. Such material exhibited superplastic elongation and it was also shown that the boundary misorientation increased to values from 10-30 degrees in extension to a strain of 100%.

While recovery takes place dynamically during the rolling, additional recovery also occurs during the reheating interval between passes.

In the Al-Mg series work, adjustment of the recovery time from four minutes to thirty minutes resulted in an improvement from the 170% range to the 500% range in elongation to fracture. For this comparison the recovery temperature was a constant 300 C. It is presumed from this result that the four minute recovery period is insufficient to provide for recovery; sub-boundaries do not form well enough to be transformed into new grain boundaries on subsequent rolling and annealing cycles [Ref. 1].

In the Al-Mg work the effect of rolling temperature also proved important. As rolling temperatures were increased the resultant material exhibited larger  $n$  values, reflected in the subsequently improved ductilities. Strength of the resultant material decreased with increasing roll temperature, offering less resistance to deformation during the superplastic process.

## B. THE STRAIN RATE SENSITIVITY COEFFICIENT

Strain rate, temperature and the microstructure of a material effect the strain rate sensitivity of the material. The relation between these variables is given by [Ref. 13]

$$\sigma_f = C \dot{\epsilon}^m \quad |_{\epsilon, T}$$

$\sigma_f$  is the flow stress

$\dot{\epsilon}$  is the strain rate

C is a material constant

and, m is the strain rate sensitivity coefficient

The strain rate sensitivity coefficient is the slope of the log. stress over the log. strain rate [Ref. 14]

$$m = \frac{d(\ln \sigma_f)}{d(\ln \dot{\epsilon})}$$

The strain rate sensitivity exponent has been shown to be a measure of resistance to local plastic instability [Ref. 14], or the ability of a material to undergo extensive elongation prior to

fracture. Superplastic materials generally exhibit  $n$  values of about 0.3 to 1.0.

Materials possessing a strain rate coefficient greater than 0.3 may still be susceptible to premature failure. If micro-cavities form in the material, coalescence can quickly result in failure in the material. And, the presence of impurities in the material may cause failure at grain boundaries. Even in cases where proper TMP is utilized, superplastic deformations may not be attainable if conditions such as these exist in the material provided.

The small grain size produced by successful TMP is essential in the development of sufficient  $n$  values. Grain boundaries act, at low temperatures, as impediments to dislocation movement. Therefore the required large mass flows involved in superplastic forming are not possible at low, or service, temperatures. At elevated temperatures, on the other hand, the increased diffusivity within the material, combined with the relatively large volume fraction of high energy grain boundary material, will assist in the large quantities of mass transport required for superplastic forming [Ref. 15].

### **C. APPLICATION OF TMP TO THE Al-2090 ALLOY**

While the theory discussed above has been successfully applied to the Al-Mg alloys, the Al-2090 material has proven more difficult. Work on 2090 has been ongoing at NPS since 1987.

Spiropoulos first investigated the applicability of thermomechanical processing methods developed for the Al-Mg series [Ref. 3]. This early work involved a matrix of TMP scheduling where aging time, reheating time, final rolling strain and rolling schedule (or reduction per pass) variables were investigated.

Noted prominently in the results of the Spiropoulos work were the following observations. Aging prior to warm rolling did not significantly affect the ductility or the strength of the material in subsequent elevated temperature testing. Increasing the reheating or recovery interval from four to thirty minutes during warm rolling resulted in enhancement of the warm temperature ductility, a decrease in flow stress, an increase in the strain rate sensitivity coefficient  $m$  and a softer and weaker material.

Transmission electron microscopy indicated that the second phase particles present in the 2090 alloy to be the  $T_1$  ( $Al_2CuLi$ ) and  $I$  phases in the short reheating interval case; in addition to the fine and evenly distributed  $T_2$  ( $Al_3Li_3Cu$ ) was present to some extent in all cases.

Ductilities achieved in the work by Spiropoulos were poor in comparison to that reached in the Al-Mg work then being completed at NPS. Spiropoulos tested at strain rates from  $6.67 \times 10^{-5} \text{ s}^{-1}$  to the  $6.67 \times 10^{-1} \text{ s}^{-1}$ . Test temperatures ranged from 300 C to 510 C.

Regis [Ref. 16] and Groh [Ref. 17] continued the investigation at NPS. Studying many of the same parameters Groh was able to make the following observations. Conducting TMP rolling in the direction of the

original plate rolled direction lead to greater ductilities. Aging 2090 and conducting 10% cold work prior to warm rolling has no effect of observed elongations.

Most important in the work of Groh is the discussion of grain boundary misorientation. It will be remembered that higher misorientation angles result in superior superplastic performance. Groh found misorientation angles as measured by transmission electron microscopy (TEM) to be no more than 2 degrees. This observation leads to the conclusion that the desired distribution of high angle boundaries is not being achieved in 2090 via the NPS TMP.

The most recent 2090 work has been that of Choudhry [Ref. 4]. Following closely the work of Groh, Choudhry attempted to demonstrate that increased rolling strain in conjunction with controlled reheating may facilitate formation of more highly misoriented boundaries and thus enhance superplasticity. In pursuit of this goal Choudhry developed a more severe rolling schedule, obtaining total reduction of 2.60, to be conducted at NPS. All rolling was conducted at 300 C and the reheating interval was fixed at 30 minutes as a result of a review of Groh's work, citing the best results in the alloy to date. Taking the premise to the extreme a schedule was developed which produced a 3.36 total rolling strain. Testing the material produced by these two thermomechanical processes demonstrated that increased rolling strain, beyond 2.50 and the introduction of higher rolling speeds, did not improve the ductilities achieved. It was also observed in this work

that the TMP employed failed to suppress cavitation at temperatures near 500 C.

The current research has thus sought other approaches to promote microstructural refinement via the continuous recrystallization reaction.



### **III. EXPERIMENTAL PROCEDURE**

#### **A. MATERIAL**

Material used for testing was provided in the form of a rolled plate with the approximate dimensions of 318mm in width, 457mm in length along the rolling direction and 38.1mm thickness. The plate was heat treated to the T8E41 temper condition.

#### **B. PROCESSING**

The thermomechanical processing (TMP) schemes used in this study closely followed the procedures utilized by Choudhry to achieve a total rolling strain of 2.60 [Ref. 4]. The modifications developed for this research are detailed below.

##### **1. Plate Sectioning and Billet Preparation**

Small billets were sectioned from the rolled plate using a band saw. The billet sections measured approximate 32mm in width by 55mm in the rolling direction. These dimensions were chosen to provide

the same amount of material after rolling as was produced by the billets used in the work of both Groh and Choudhry [Refs. 4 & 17]. Where Groh and Choudhry sectioned after forging, the billets in this work were sized for processing as single pieces. The rolling direction of the parent plate was retained as the principle direction for eventual rolling in the sectioned billets.

## **2. Solution Treatment and Forging**

Solution treatment was conducted in a furnace heated to 540 C. This temperature is well above the solvi for both the  $T_1$  and  $T_2$  phases, but below the solvus for  $Al_3Zr$ . Initial solution treatment prior to forging was for eight hours after which the billets were forged in the short transverse direction, reducing their height to 25.4mm. Forging was conducted between platens heated to 480 C, the maximum allowable temperature of the platens, in a Baldwin-Tate-Emery Universal testing machine. After forging the billets were immediately returned to the furnace for an additional four hours of further solution treatment before water quenching.

## **3. Rolling**

All rolling was conducted at the Naval Postgraduate School utilizing a laboratory rolling mill having a maximum roll opening of

25mm. The mill's rolls measure 11.1cm in diameter and were manually cleaned by hand polish prior to each pass of the material. The rolls were not heated. To maintain approximately isothermal conditions techniques were developed to quickly transfer the material from the annealing furnace to the rolls. Time spent by the material on the mill entry table was viewed as especially critical as the table is thermally massive and acts as a heat sink. Such time was minimized to preserve material temperature during the rolling process.

At this juncture in the TMP, important departures from previously attempted rolling schemes were instituted. The goal remains to promote the continuous recrystallization process. The progression of rolling and recovery cycles is designed to introduce dislocations in the former, and provide for their recovery in the latter; with the ultimate goal being the creation of highly refined grain structure. As outlined above, resultant grain size should be small and sufficiently misoriented boundaries misorientations are desired.

For every rolling condition used in this study the recovery temperature was maintained at 300 C. In each scheme the recovery time at temperature was maintained at 30 minutes, the time found most advantageous in earlier work and NPS. The temperatures at which the material was stabilized just prior to rolling became the variable of interest. In all cases the first five passes were conducted with the material at the 300 C recovery temperature. The final five passes of the lower temperature series were conducted at 250 and 150 C, respectively. It was determined that the material could not be

successfully rolled to a total strain approaching 2.60 at temperatures less than 150 C, marking the lower temperature boundary for the chosen rolling scheme. The lower rolling speed was used throughout the processing.

Table I contains the rolling schedule of reductions followed and is identical in each of the three temperature profiles. For comparison purposes the schedule used in the most recent previous work is also provided [Ref. 4]. It will be quickly noted that the only difference between the two schedules is in the final pass.

**Table I: ROLLING SCHEDULE OF REDUCTIONS:  
COMPARISON OF PREVIOUS WORK TO CURRENT WORK.**

---

Rolling Pass	Thickness	
	Previous (mm)	Current (mm)
0	25.4	25.4
1	22.9	22.9
2	20.3	20.3
3	17.8	17.8
4	15.2	15.2
5	12.7	12.7
6	9.5	9.5
7	6.2	6.2
8	4.3	4.3
9	2.5	2.5
10	1.98	1.76

---

A greater reduction is taken in the final pass, in this the most recent work, so that the rolling strain rate as described by Harris

[Ref. 18] can be characterized as continuously increasing. The equation for rolling strain rate is:

$$\dot{\epsilon} = v_r \left( \frac{1}{R\Delta h} \right)^{1/2} \ln (h_o/h_f)$$

where  $v_r$  is the tangential velocity of the roll surface,  $r$  is the roll diameter, and the  $h$  values are the thickness measurements of the material being rolled. This fact is graphically illustrated in Figure 1. On completion of the final rolling pass the material was water quenched.

#### 4. Sample Preparation

After rolling the material was machined into tensile samples conforming to Figure 2. The tensile test samples were prepared such that the test axis was parallel to the rolling direction. In the case of the third temperature profile, (150 C on the final five passes) a limited number of samples was the result of severe cracking along the sides of the material running the length of the final piece.

# WARM ROLLING STRAIN RATE

NOMINAL NPS SCHEDULES

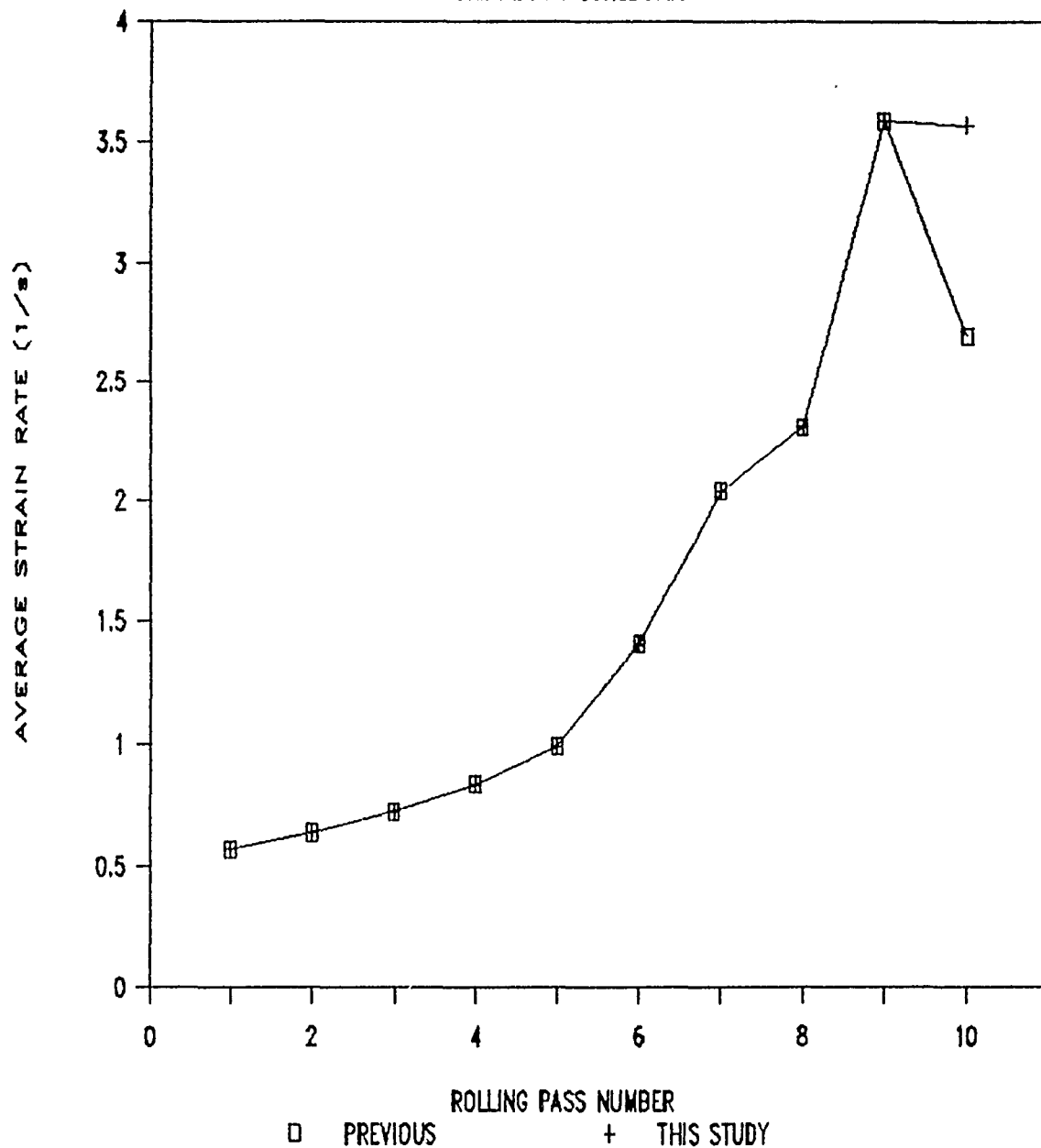
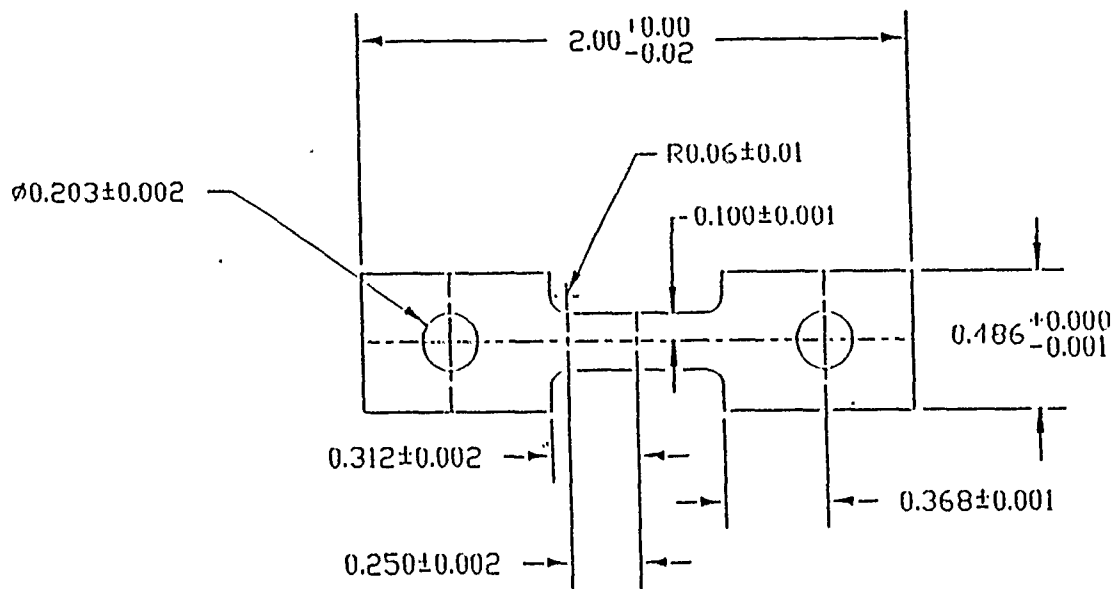


**Figure 1.** Plot of Warm Rolling Strain Rate vs. Rolling Pass: Depicting the Increased Warm Rolling Strain Rate used during the Final Pass of this Study over that used in Previous Work.

# TENSILE SAMPLE GEOMETRY



Note: All dimensions are in inches.

**Figure 2.** Tensile Test Sample Dimensions. The Effective Gage Length is 0.5 Inches in All Cases while the Thickness is a Function of Final Rolling Strain.

### C. TESTING

Selection of the testing matrix also followed closely the most recent work conducted at NPS. The first series nearly replicated the test coverage of Choudhry. Strain rates between  $6.67 \times 10^{-5} \text{ s}^{-1}$  and  $6.67 \times 10^{-2} \text{ s}^{-1}$  were employed and temperatures of 300, 350, 370, 400, 450 and 500 C composed a complete test matrix. Reduced test matrices were used in the second and third test series to concentrate efforts and conserve test samples.

Testing was conducted on an Instron model TT-D testing machine equipped with a Marshall three zone, clam-shell furnace to heat the specimens to test temperature. Tensile specimens were placed into specially prepared grips which had been preheated to temperature, reducing the time required to heat the specimen to approximately 35 minutes. The specimen and grips were instrumented with of thermocouples to assist in providing accurate temperature control.

A stripchart recorder produced load versus time recordings autographically. These recording were converted to true stress versus true strain by computer program. The program compensated for the decreases in true strain rate with increasing strain. Plots were produced by commercial software on the NPS mainframe computer. The conversion program appears as Appendix 1.



#### D. METALLOGRAPHY

Optical microscopy was conducted on material in the as-rolled condition and on selected samples after tensile testing. In each case the samples were cold mounted and mechanically polished. Diamond paste wheels utilizing 6, 3, and 1 micron diamond paste were used in succession prior to final polishing using cerium oxide slurry.

The rolling direction was preserved throughout the current work. Descriptions of the microstructure is simplified by this fact. Observations of the microstructure, as cited in this thesis, comply with the following practice. The surface plane view contains the rolling direction and the long transverse direction, and is normal to these two directions. The short transverse plane is the normal to the long transverse and the short transverse (or through thickness direction). Finally the long transverse view is the plane containing the rolling direction and the short transverse direction.

Specimens were etched in Kellers reagent for 10-20 seconds followed by immersion in concentrated nitric acid ( $\text{HNO}_3$ ) for 3-5 seconds. If necessary to improve contrast, the final polish and etch was repeated. After each phase of the etching cycle the samples were rinsed in ethanol and dried [Ref. 4].

A Zeiss ICM 405 optical microscope equipped with a 35mm camera was used for the metallography. Film, negatives and prints were manually developed and prepared.

#### IV. RESULTS AND DISCUSSION

##### A. MICROSTRUCTURAL CONDITION PRIOR TO ROLLING

Extensive examination of the microstructural condition of the Al-2090 was conducted by Groh, making use of both optical and transmission electron microscopy (TEM). This work attempted to outline the influence of process variables on the resultant microstructure. [Ref. 17]

The TMP sequence through solution treatment, upset forging and heating prior to rolling creates an inhomogeneous, coarse-grained microstructure. Both inter-granular and intra-granular precipitates are present. Grains tend to remain aligned parallel to the rolling transverse direction of the original plate. [Ref. 17]

Investigation by TEM revealed the grain boundaries to be decorated with the  $T_2$  phase. Within the grain interiors the precipitated phase is  $T_1$ . With the precipitate ( $T_2$ ) on the grain boundaries, there is a resulting precipitation free zone (PFZ) where  $T_1$  is absent and then an interior region where the  $T_1$  has formed. [Ref. 17]

## B. MICROSTRUCTURAL CONDITION AFTER ROLLING

Optical micrographs were obtained for each of the rolling temperature sequences. As-rolled material was sectioned to reveal the rolled surface and both long and short transverse surfaces. The TMP produced a fine microstructure for each of the three rolling conditions. The results of the optical microscopy are presented in Figures 3 through 5. These views are of the material rolled at 150 C in the final five passes, but are representative, at the level of optical microscopy, of all rolled conditions in this study and show a fine distribution of precipitated second phase particles in a matrix. This uniformly fine microstructure is nearly identical, again at the optical level, to that achieved by Choudhry [Ref. 4] and Groh [Ref. 17]. The second phase most likely consists of  $T_2$  precipitates residing at triple junction in the microstructure as determined in Groh's TEM work [Ref. 17].

It is difficult to distinguish between inclusions and microvoids in the micrographs accompanying this chapter. Careful observation of the microstructure, where the focus can be adjusted to assist in identification, resulted in the observations made. To assist the reader the following general observations are provided.

Inclusions appear to exhibit an equiaxed morphology.

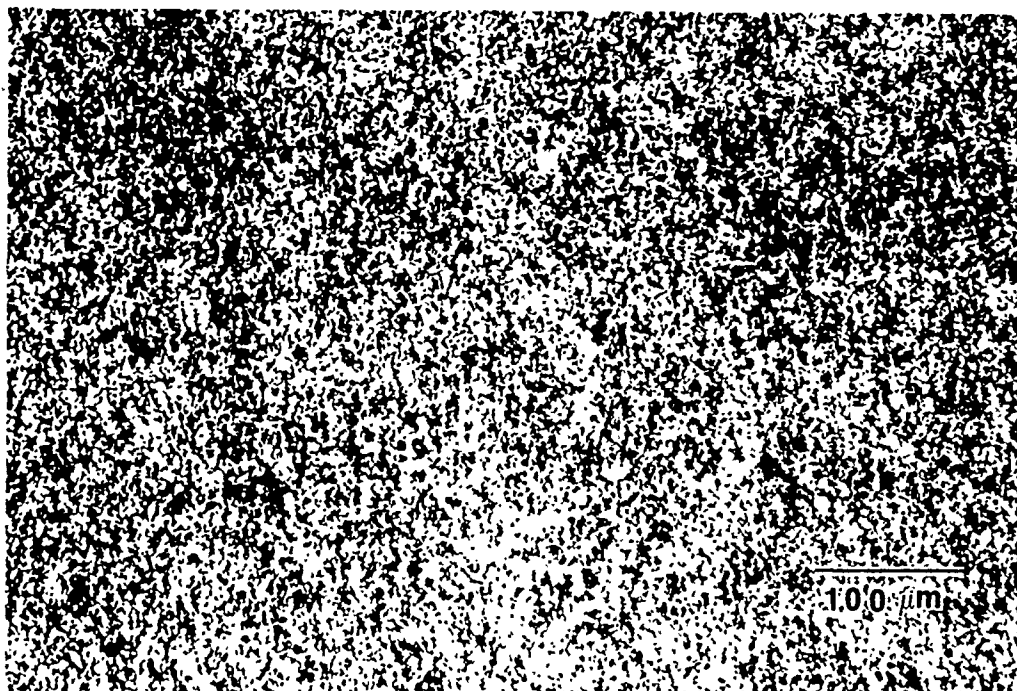
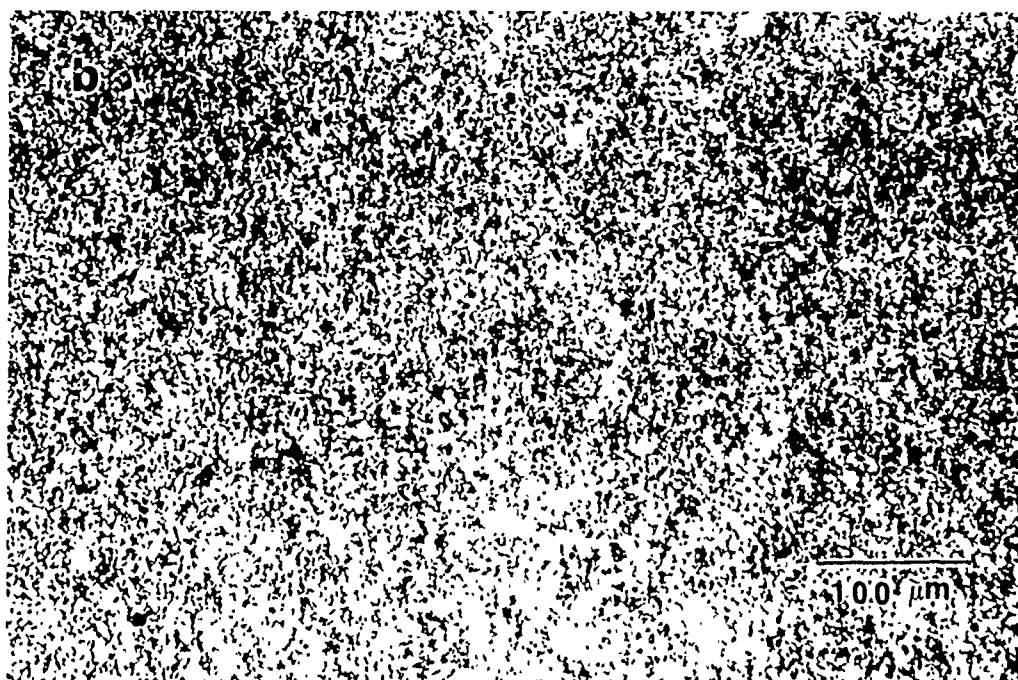
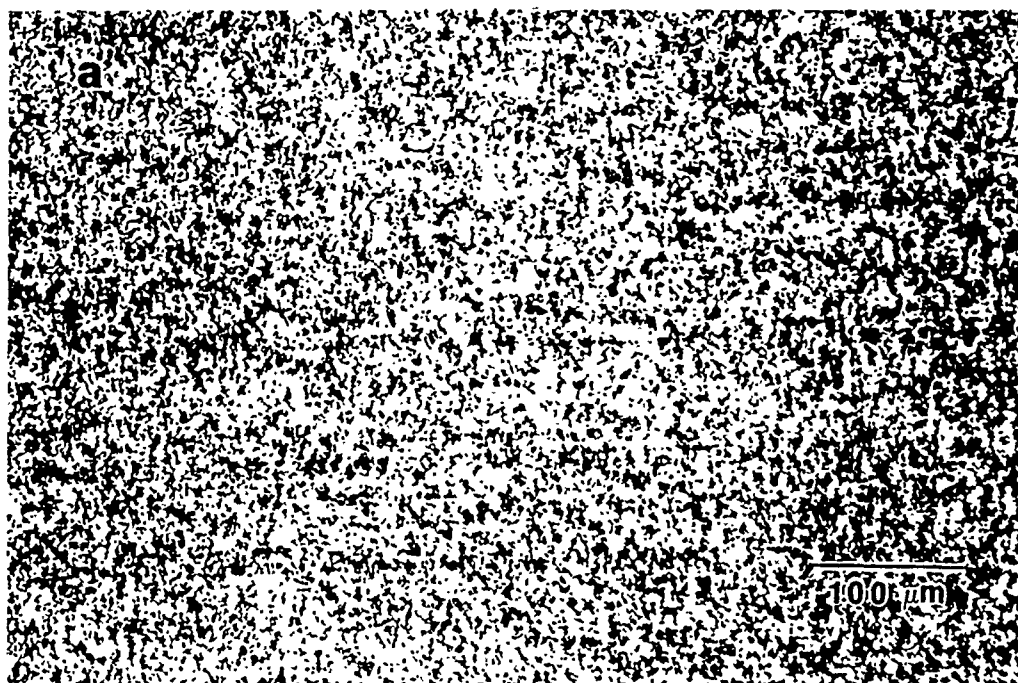
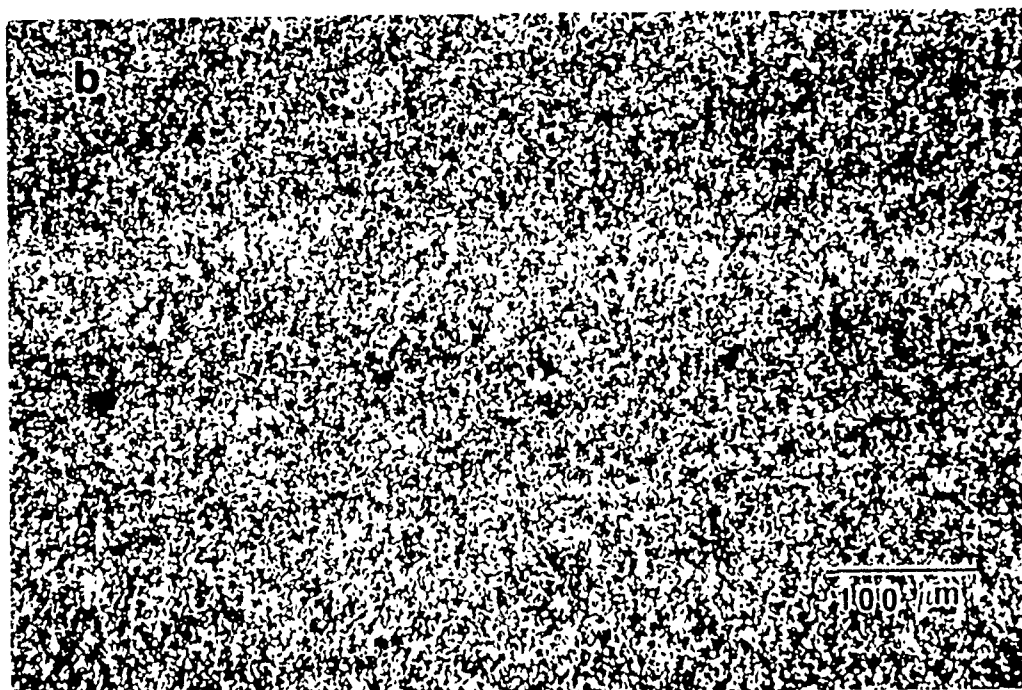
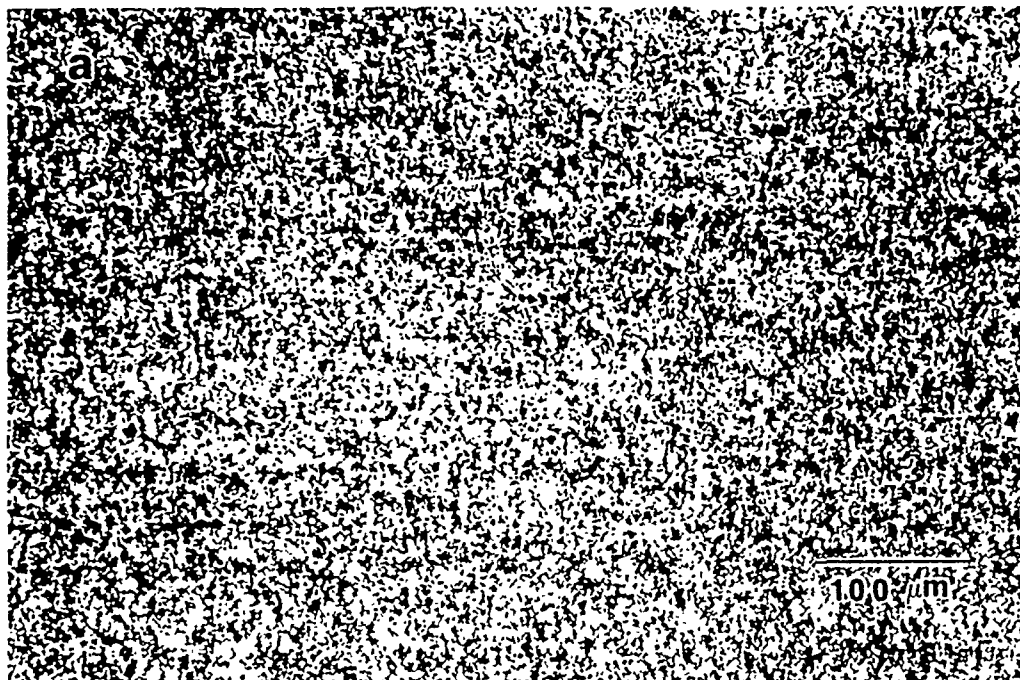


**Figure 3.** Surface Micrograph of Material Rolled at 150 C for Final Five Passes. Scattered Inclusion Content Discernable. View is Representative (at optical level) of Surface Condition for each Rolling Scheme Covered in this Study.



**Figures 4 (a) and (b).** Long Transverse Optical Micrographs of Material Rolled at 150 C in Final Five Passes. Figure 4 (a) is Low in Inclusion Content, While 4 (b) Contains a Considerable Number of Inclusions Visible in the Banding.



**Figures 5 (a) and (b).** Short Transverse Optical Micrographs of Material Rolled at 150 C in Final Five Passed. Figure 5 (a) is Low in Inclusion Content While 5 (b) Contains a Considerable Number of Inclusions Visible in the Banding.

Microvoids, on the other hand, can be distinguished by the visible triple points left behind as grain boundary sliding allows material to be pulled away. Larger collections of microvoids created in this manner are strung together and are primarily found to lie in the direction of the microstructural banding.

Varying inclusion content is discernable upon examination of the as-rolled specimen. The degree of variation in inclusion content is illustrated by comparison of the short- and long- transverse planes as represented by Figures 4 and 5. The rolling plane, as viewed in the Figure 3 indicates a continuous distribution of inclusions.

### C. RESULTS OF MECHANICAL TESTING

The primary objective enroute to improving the performance of the alloy, it will be remembered, was to introduce additional dislocations in support of the CRX mechanism. The variables in previous work included rolling speed, total rolling strain [Ref. 4], recovery period, and recovery temperature [Refs. 3 & 17]. In this work, as outlined above, the processing prior to testing was modified only slightly from that of Choudhry. As described in the experimental procedure, the first roll scheme differed only in the reduction taken in the final pass. The next two schemes contained the added dissimilarity of having reduced rolling temperatures while annealing between rolling passes was still carried out at 300 C.

Microstructure, at the optical level, reveals a very similar structure to that previously reported as resulting from the NPS process scheme developed by Groh and Choudhry.

Moderate improvements in ductilities relative to those of previous work [Refs. 3, 4, 16, & 17] were obtained in the temperature range covering 350 to 450 C. Again in keeping with previous results, the strain rates producing the greatest elongations were the middle two rates of these covered by testing. A summary of the elongation results for the three rolling schemes is provided in Table 1 of Appendix 1. Results of the testing are also summarized in Figures 6 through 8.

The first set of results reported here are for the 300 C roll series and represent the effect of increasing the reduction taken in the final pass through the mill, while maintaining the rolling temperature at the recovery temperature. Elongations as result of this small modification are slightly improved over those previously obtained. It is believed that this is a result of maintaining a higher strain rate during the TMP, and thereby promoting CRX by increasing the dislocation density available for the CRX process.



# Ductility vs. Tensile Test Temperature

300 C Temperature Roll Series

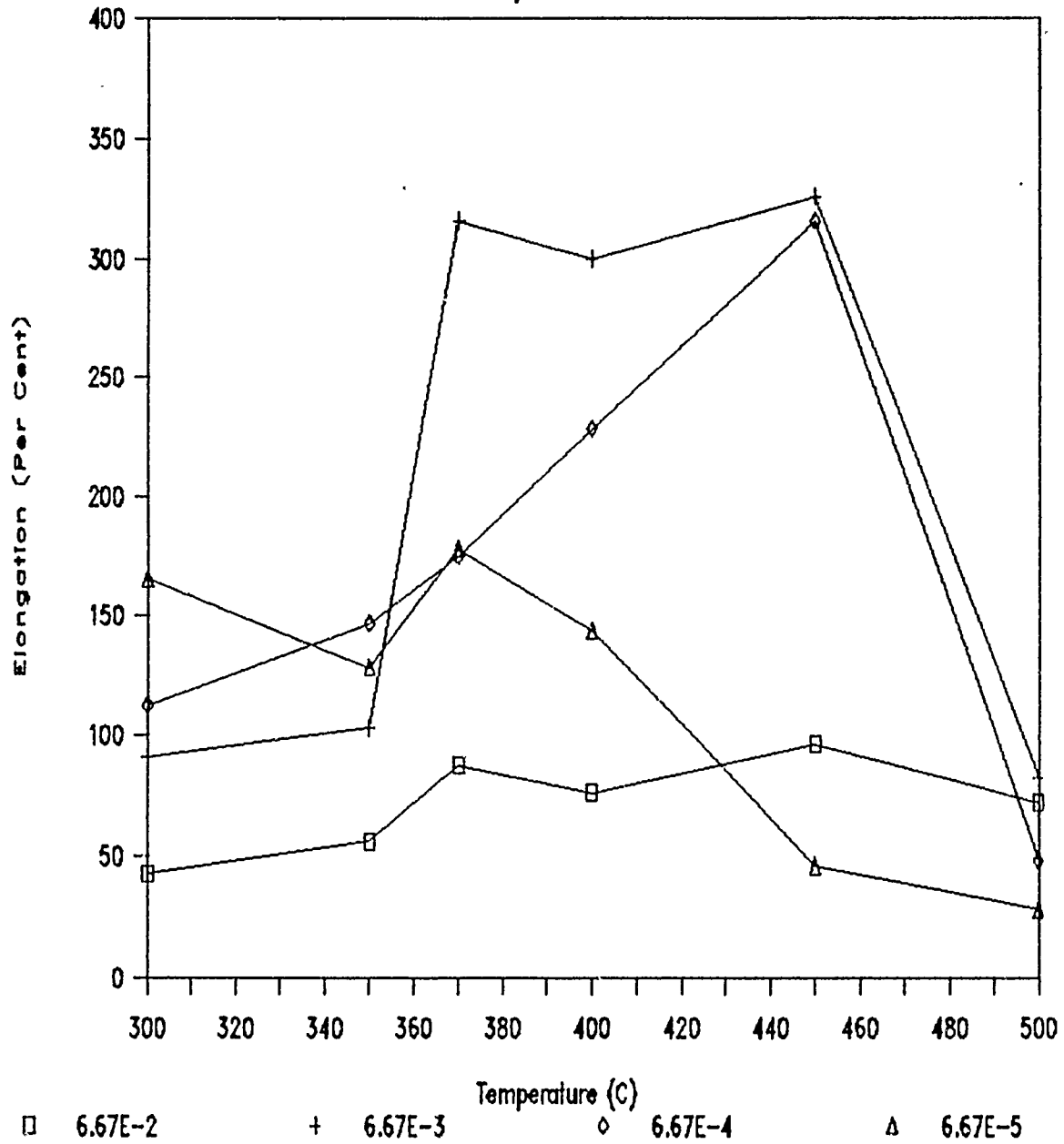


**Figure 6.** Ductility vs. Tensile Test Temperature for Material Rolled at 300 C.

# Ductility vs. Tensile Test Temperature

250 C Temperature Roll Series

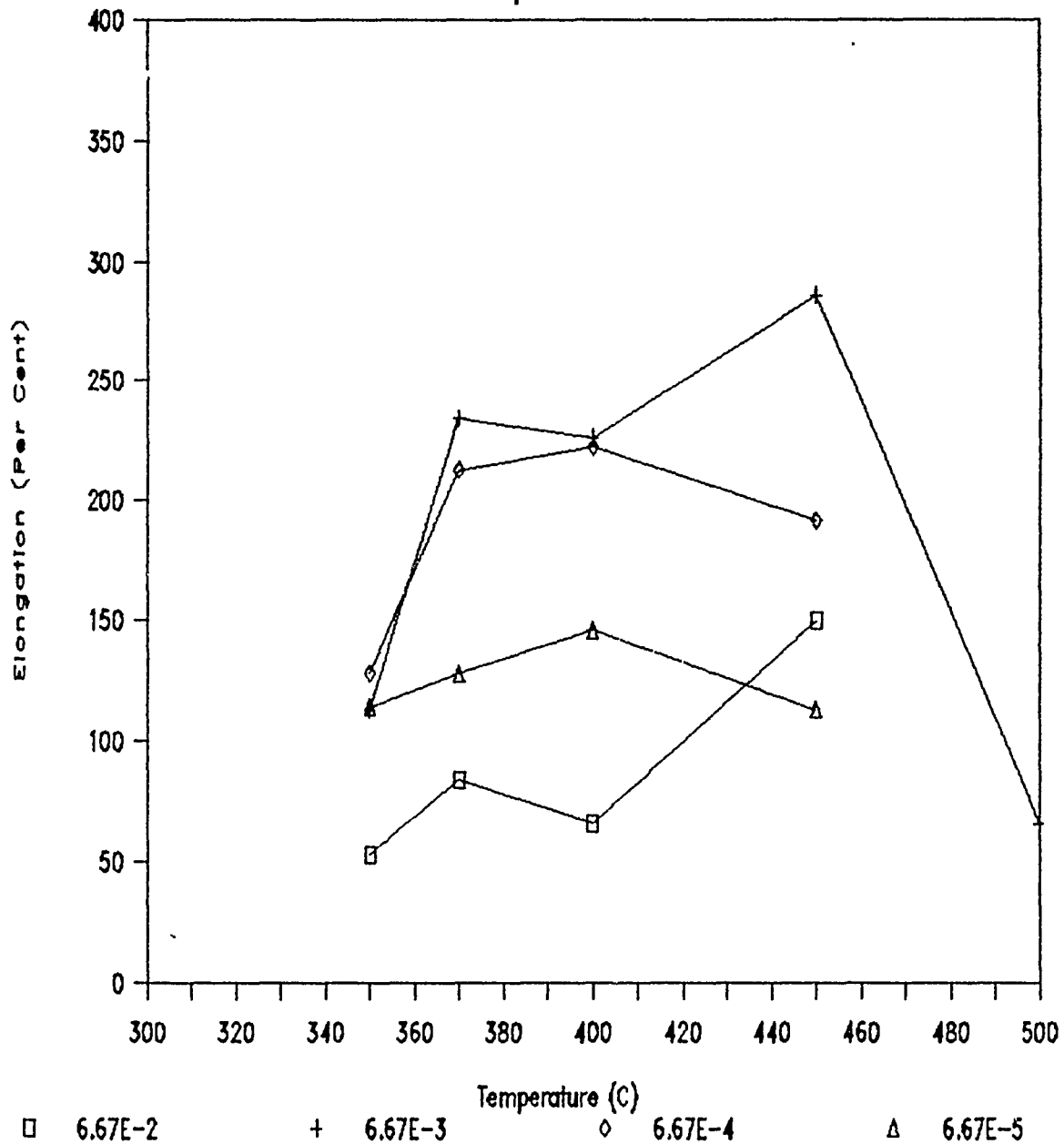


**Figure 7.** Ductility vs. Tensile Test Temperature for Material Rolled at 250 C in the Final Five Rolling Passes.

# Ductility vs. Tensile Test Temperature

150 C Temperature Roll Scheme Series

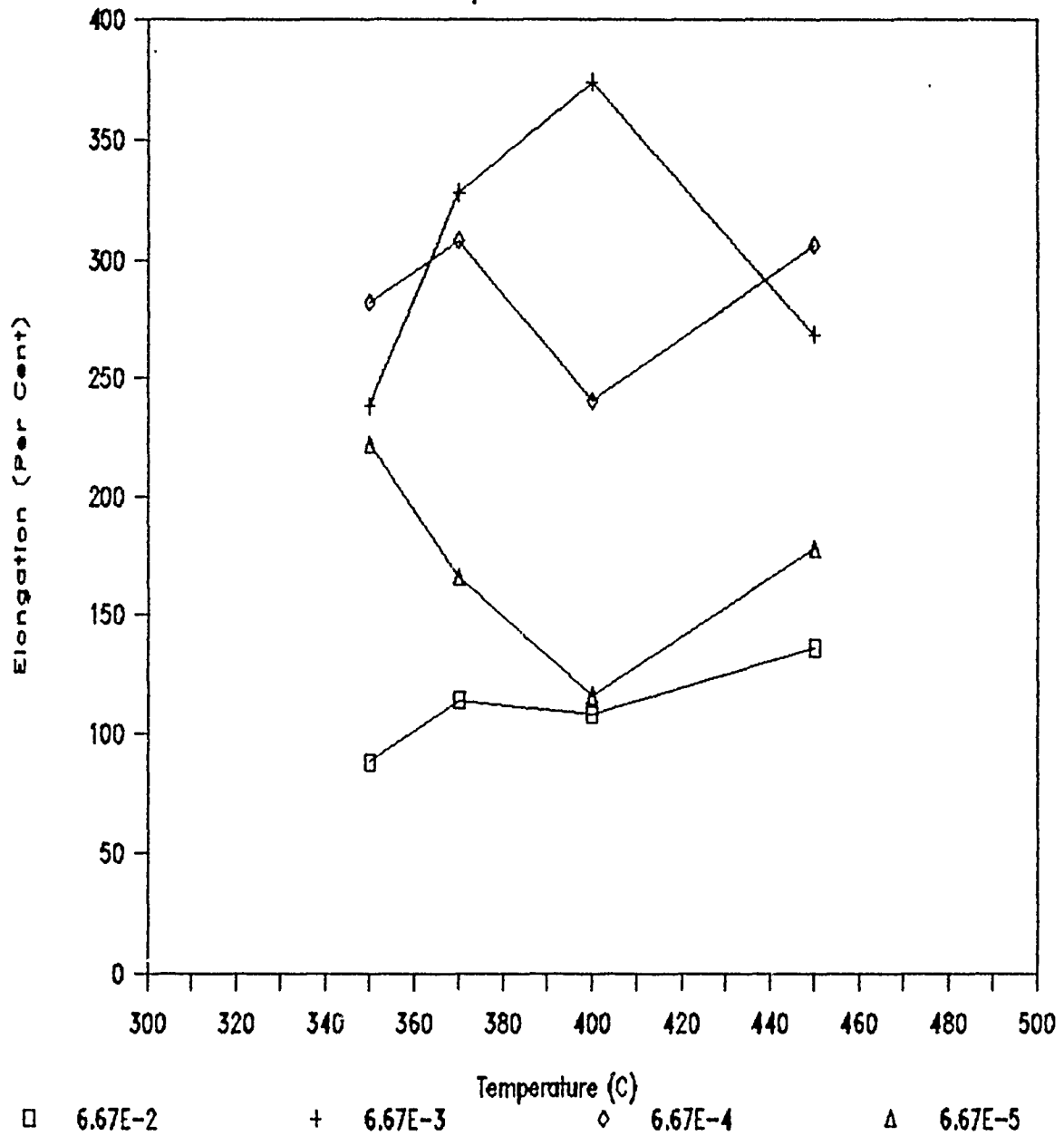


**Figure 8.** Ductility vs. Tensile Test Temperature for Material Rolled at 150 C in the Final Five Rolling Passes.

To increase still further the number of dislocations introduced into the material the next set of billets was stabilized at 250 C prior to each of the final five rolling passes. Results of this again are only moderately improved over those obtained by Choudhry and were in fact less than the elongations already achieved by maintaining a rolling temperatures of 300 C. The fifty degree difference between by these two schemes may, in retrospect, have little effect and the data reflect only the statistical range of results which might be expected in the process temperature range.

The final scheme, involving the stabilization of the material at 150 C prior to the last five rolling passes, likely results in a significant increase in dislocation generation. This was evident during the rolling where severe cracking along the sides of the material resulted during the final mill pass. This represents the limit of deformation and warm work the alloy can sustain under this roll reduction schedule but did result in reasonable improvement in elongation values. An elongation of 374% was achieved at 400 C and a strain rate of  $6.67 \times 10^{-3} \text{ s}^{-1}$ . This represents a considerable improvement over previous work [Refs. 4 & 17].

The 150 C rolling schedule also provided improvement at the slower strain rate of  $6.67 \times 10^{-4} \text{ s}^{-1}$  where a broad temperature plateau in ductility near 300% is evidenced. This represents improvement over previous results in that both the elongations and the range of favorable results is extended to 450 C.

Flow stresses measured at a true strains of 0.1 mm/mm are presented graphically for each TMP in Figures 9 through 11. These data indicate slightly reduced flow stresses in the series deformed at  $6.67 \times 10^{-4} \text{ s}^{-1}$  and  $6.67 \times 10^{-3} \text{ s}^{-1}$ , especially at higher temperatures, when compared to previous research. This marginal reduction in flow stress is to be expected in light of the correspondingly moderate improvement in ductility already seen in the previous set of Figures.

A historical review is represented by Figures 12 & 13. The best results (at the middle strain rates and with the most similar TMP) reported by NPS researchers working with Al-2090 are summarized. From these two Figures steady improvements can be inferred.

When this historical summary of the NPS work is considered in the light of results published by others elsewhere, a considerable difference in the nature of the two sets of results is immediately apparent. While the elongation Figures for NPS work drop precipitously as temperature is increased above 450 C the results for others indicate superior results at temperatures above 450 C.

It should be recognized that the TMP developed at NPS has improved low temperature ductilities, its intended goal. It remains to be explained why different approaches to the development of a TMP result in different elongation profiles with respect to testing temperature.

# Flow Stress At Strain Of 0.1 mm/mm

300 C Temperature Roll Series

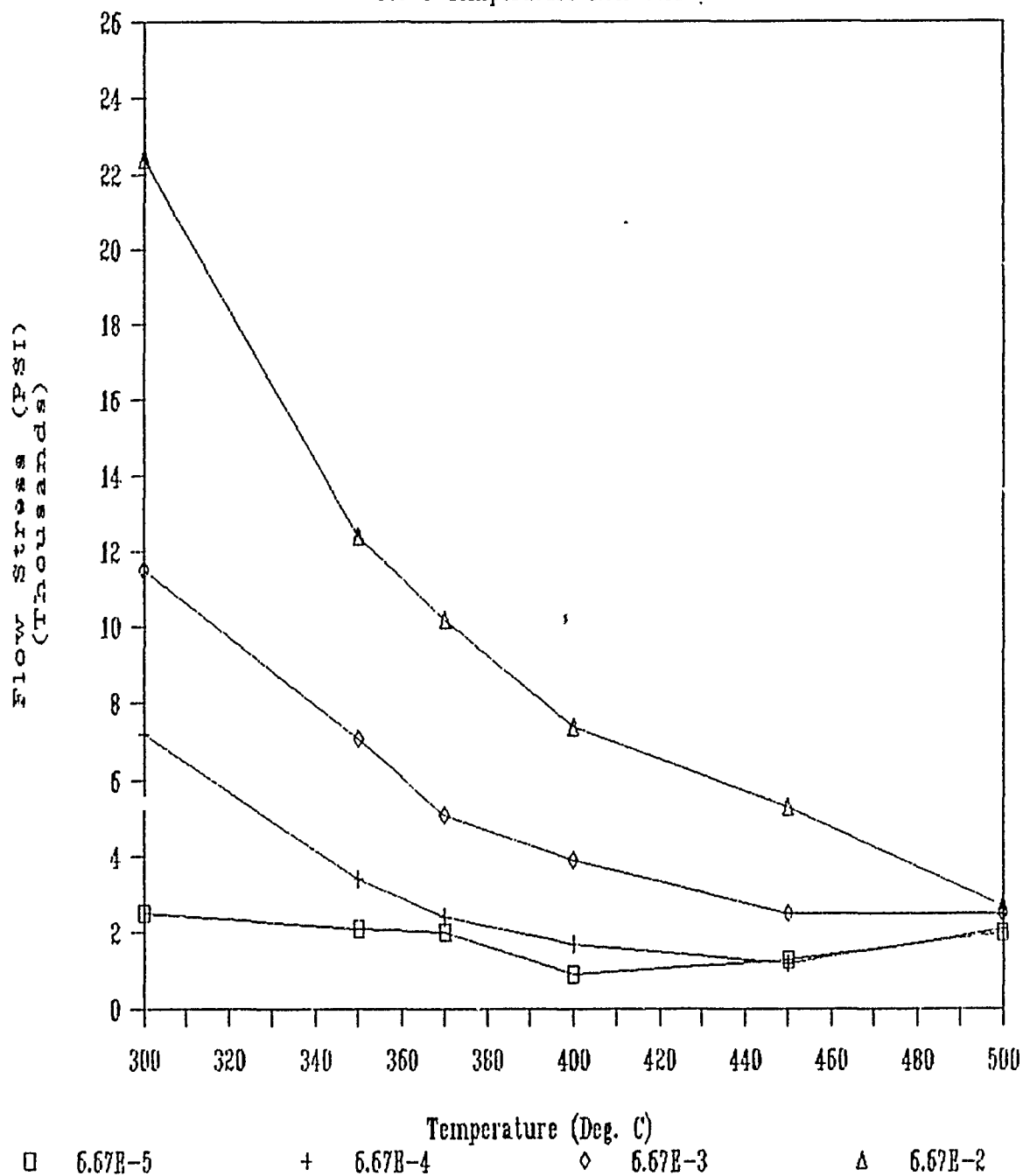


**Figure 9.** Flow Stress at True Strain of 10% vs. Test Temperature for Material Rolled at 300 C.

# Flow Stress At Strain Of 0.1 mm/mm

250 C Temperature Roll Series

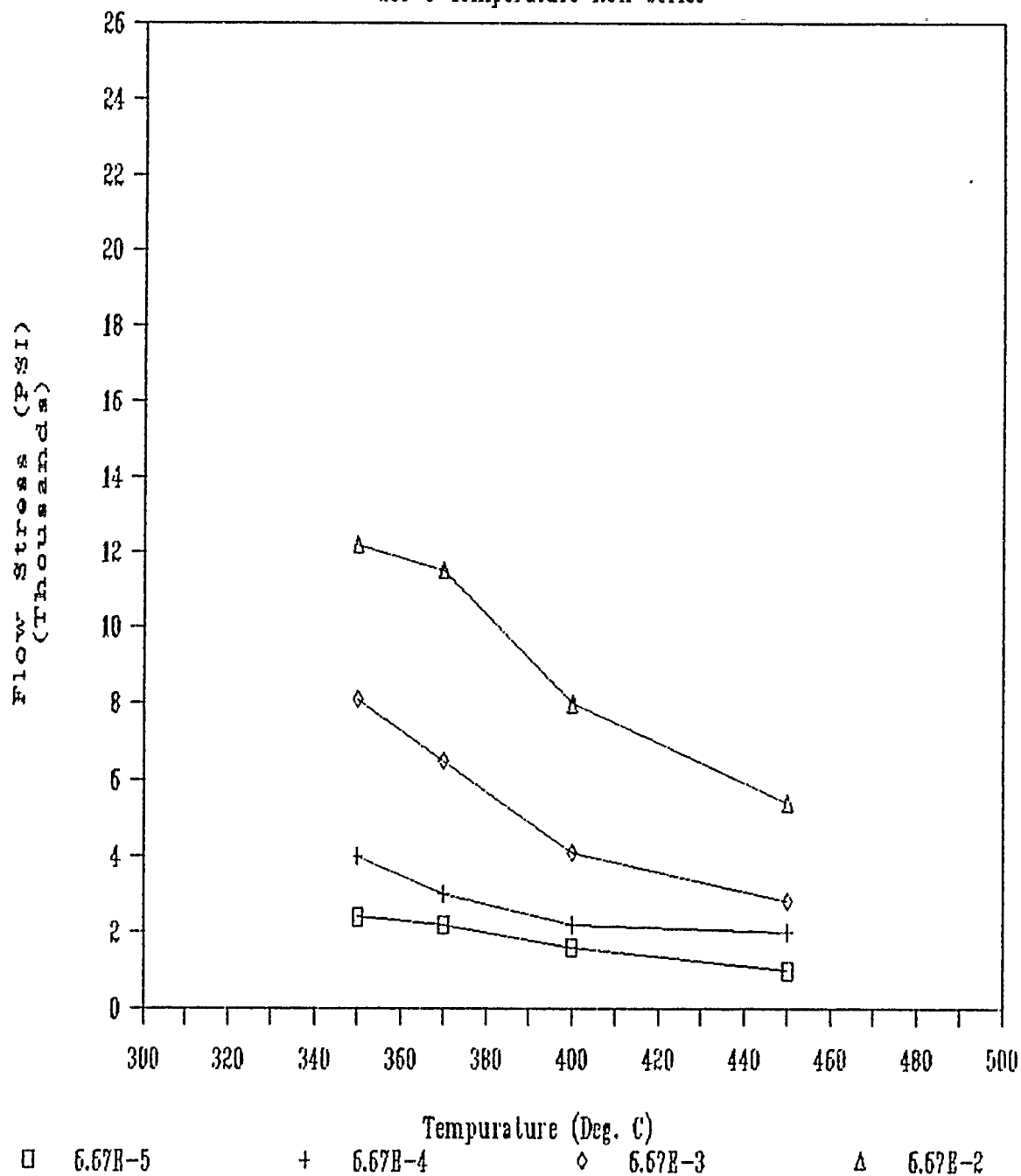


**Figure 10.** Flow Stress at True Strain of 10% vs. Test Temperature for Material Rolled at 250 C for the Final Five Rolling Passes.

# Flow Stress At Strain Of 0.1 mm/mm

150 C Temperature Series Series

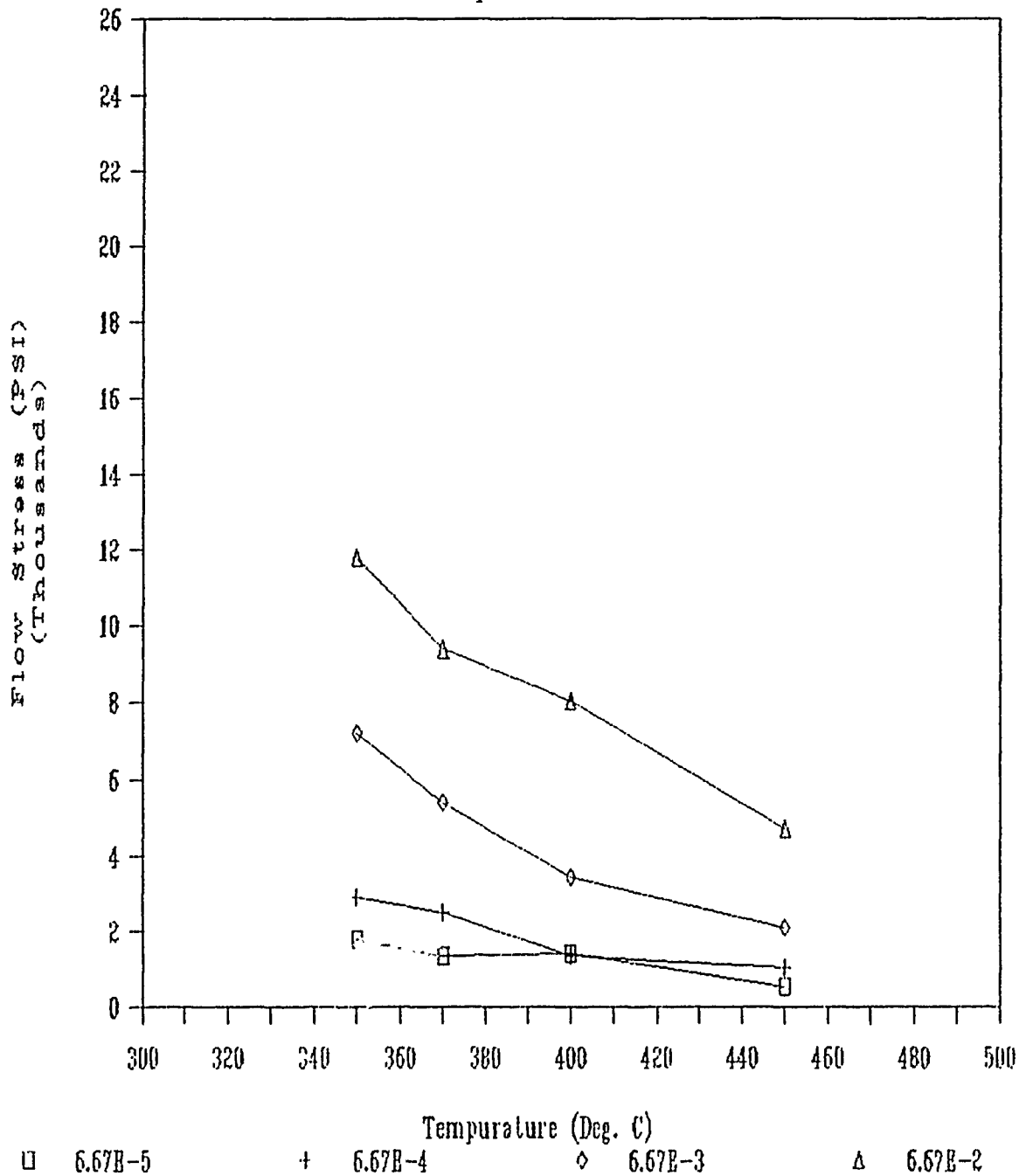


**Figure 11.** Flow Stress at True Strain of 10% vs. Test Temperature for Material Rolled at 150 C for the Final Five Rolling Passes.



# RESULTS COMPARISON

6.67x10<sup>-3</sup>, STRAINRATE

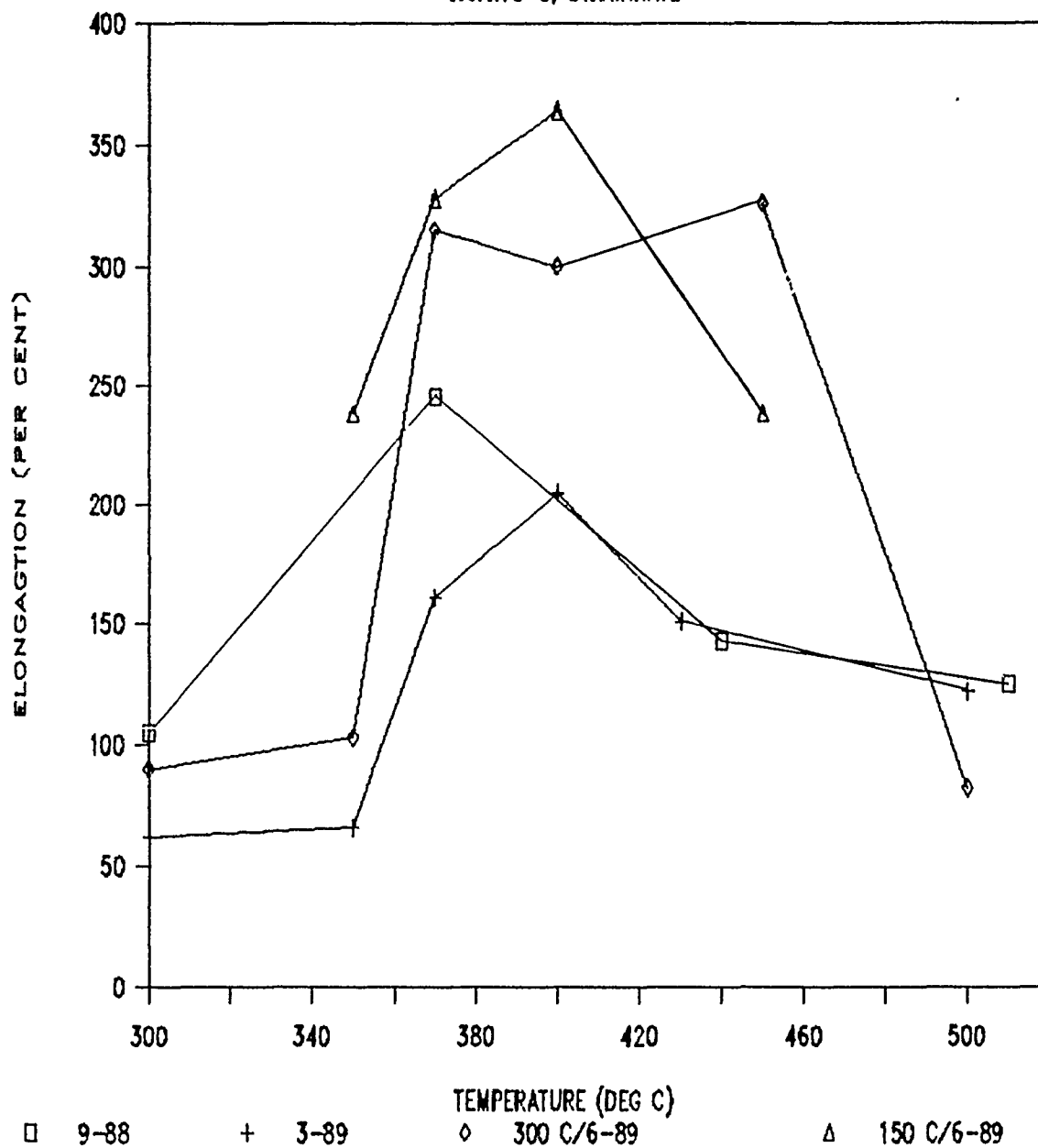


**Figure 12.** Historical Overview of Results of Testing at a Strain Rate of  $6.67 \times 10^{-3} \text{ s}^{-1}$ , Depicting a General Trend Toward Improved Elongation as a Result of Refinements to Thermomechanical Processing (TMP).

# RESULTS COMPARISON

6.67x10<sup>-4</sup>, STRAINRATE

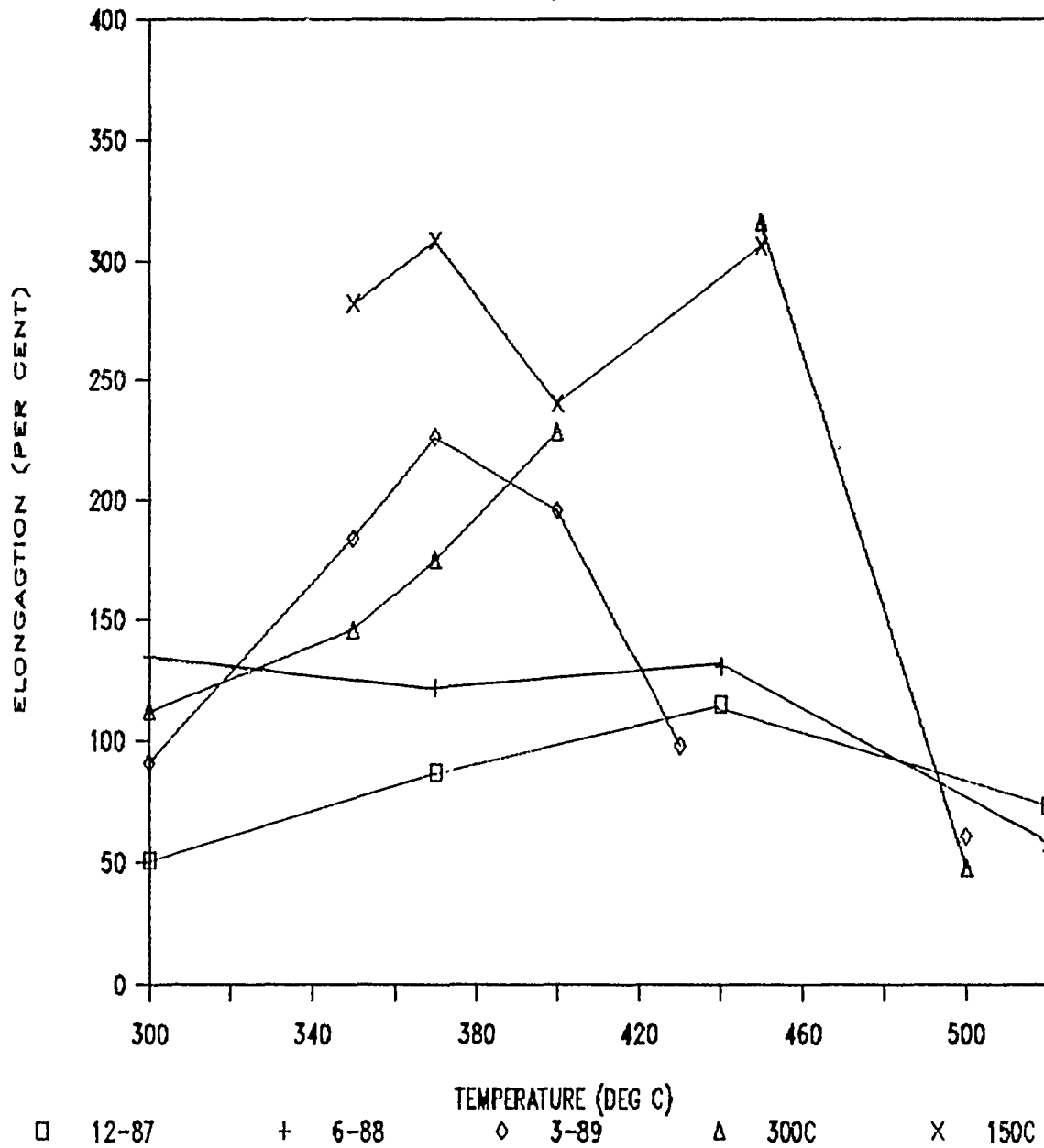


**Figure 13.** Historical Overview of Results of Testing at a Strain Rate of  $6.67 \times 10^{-4} \text{ s}^{-1}$ , Depicting a General Trend Toward Improved Elongation as a Result of Refinement to Thermomechanical Processing (TMP).

#### D. CONDITION OF MICROSTRUCTURE AFTER DEFORMATION

Samples from the final rolling scheme (150 C), tested at a temperature of 400 C and strain rate of  $6.67 \times 10^{-3} \text{ s}^{-1}$  with an elongation of 374%, and also at a temperature of 370 C and strain rate of  $6.67 \times 10^{-4} \text{ s}^{-1}$  with an elongation of 308%, were sectioned and prepared for optical microscopy.

Long transverse and surface optical micrographs of the gage section of the 400 C,  $6.67 \times 10^{-3} \text{ s}^{-1}$  specimen are shown in Figures 14 and 15, respectively. Both of these views reveal a fine microstructure and indicate that a slight coarsening has occurred during testing at elevated temperature.

Just discernable in the gage section (surface and long transverse) micrographs is a fine distribution of microvoids. Figure 16 is a low power micrograph of the surface fracture tip provided to demonstrate the absence of extensive microvoid coalescence, even to the point of fracture. The photomicrograph of the long transverse and surface gage sections reveals resistance to cavitation, an important requirement for successful superplastic forming. The micrograph depicting the surface view of the fracture area is practically devoid of cavitation. This is a positive development reflecting the ability of the alloy to resist cavitation and incipient failures which result from this mechanism in superplastic forming.

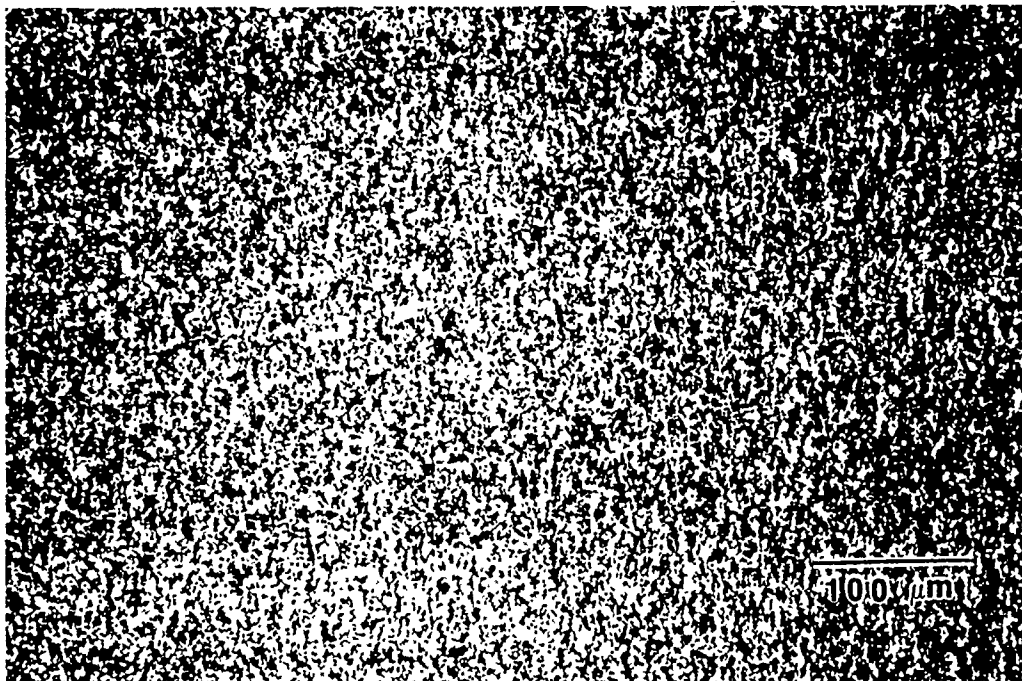


**Figure 14.** Long-Transverse Grip Section Micrograph of the Specimen Rolled at 150 C and Tested at 400 C and Strain Rate of  $6.67 \times 10^{-3} \text{ s}^{-1}$ , Exhibiting an Extremely Fine Distribution of Second Phase Particles in a Matrix.

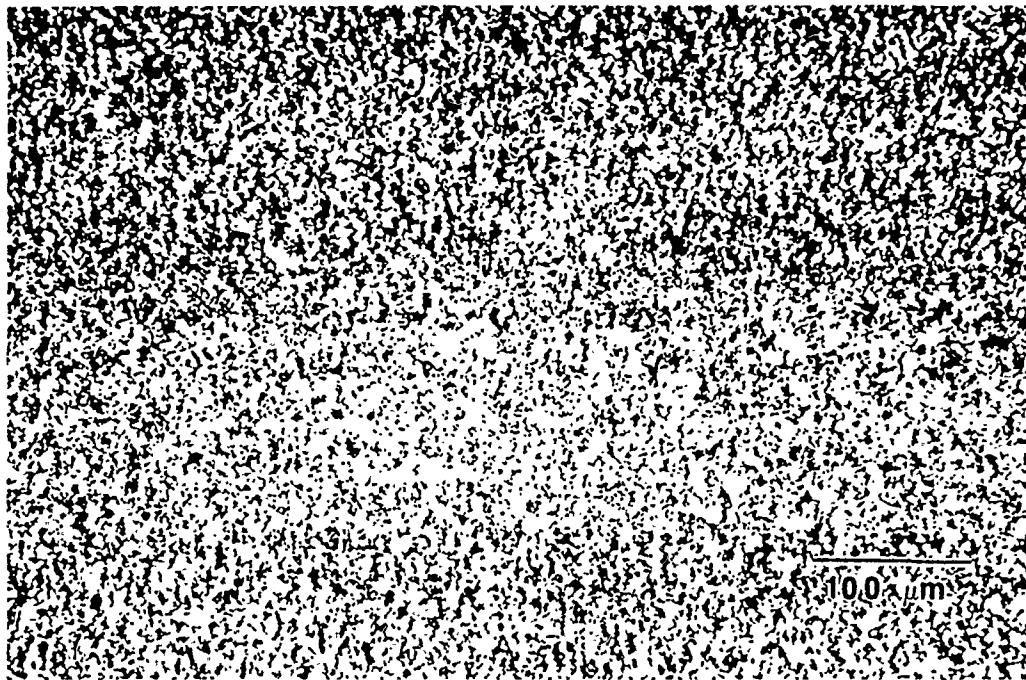


**Figure 15.** Micrograph of the Long-Transverse Gage Section Shown in Comparison to Figure 14, Exhibiting Retention of the Fine Dispersion of the Second Phase, and only Slight Cavitation.

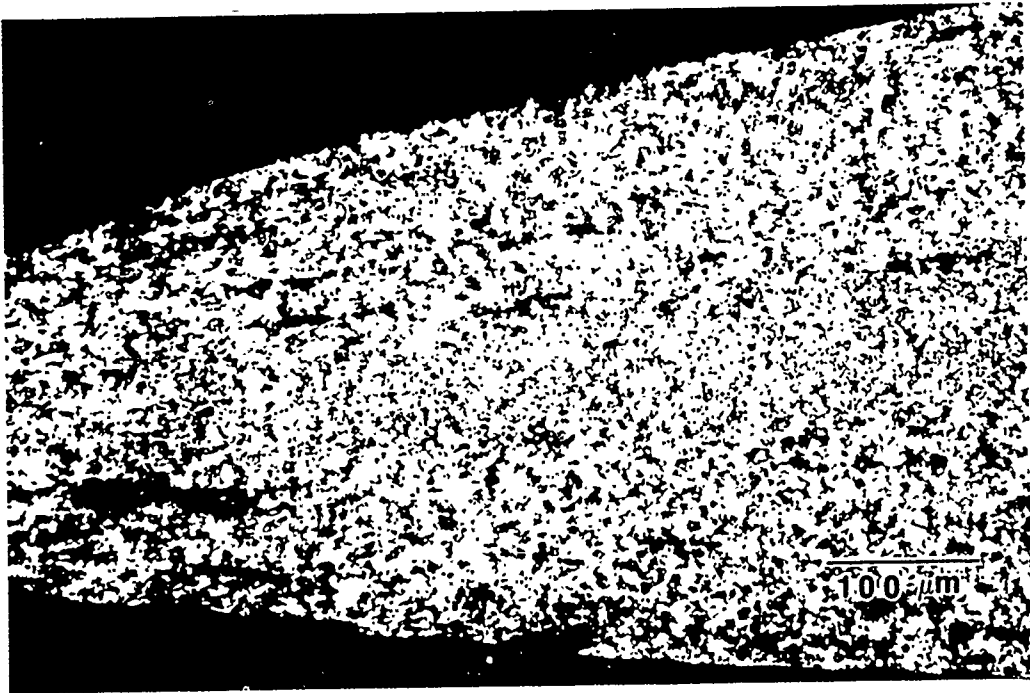


**Figure 16.** Micrograph of the Fracture Tip of the Specimen attaining 375% Elongation, Illustrating Limited Cavitation in the Unnecked Section, and Increasing Cavitation and Coarsening in the Vicinity of the Fracture Tip.

The optical micrographs from the sample tested at 370 C and  $6.67 \times 10^{-4} \text{ s}^{-1}$ , Figures 17 and 18, represent the long transverse gage section and the accompanying grip section. These micrographs exhibit microstructure similar to that observed in the 400 C,  $6.67 \times 10^{-3} \text{ s}^{-1}$ , specimen indicating the broad temperature and strain rate range over which improved microstructural results have been obtained by the TMP employed.

Close examination of the long transverse gage section of this second specimen, Figure 18, reveals larger microvoids than encountered in the sample which attained 374% elongation. The increased size of the microvoids most likely contributed to the earlier failure of the second sample. A primary candidate to cause such a premature onset of necking and eventual failure is the inhomogeneous distribution of inclusions as noted in comparison micrographs for the as-rolled condition. Thus, the near 20% difference in the elongations recorded for these two samples likely is representative of the apparent scatter in the data.

#### **E. EVALUATION OF STRAIN RATE COEFFICIENTS**

Strain rate coefficients,  $m$ , have been computed for the material prepared and tested during the course of this work. The values achieved as a result of modification to TMP are provided

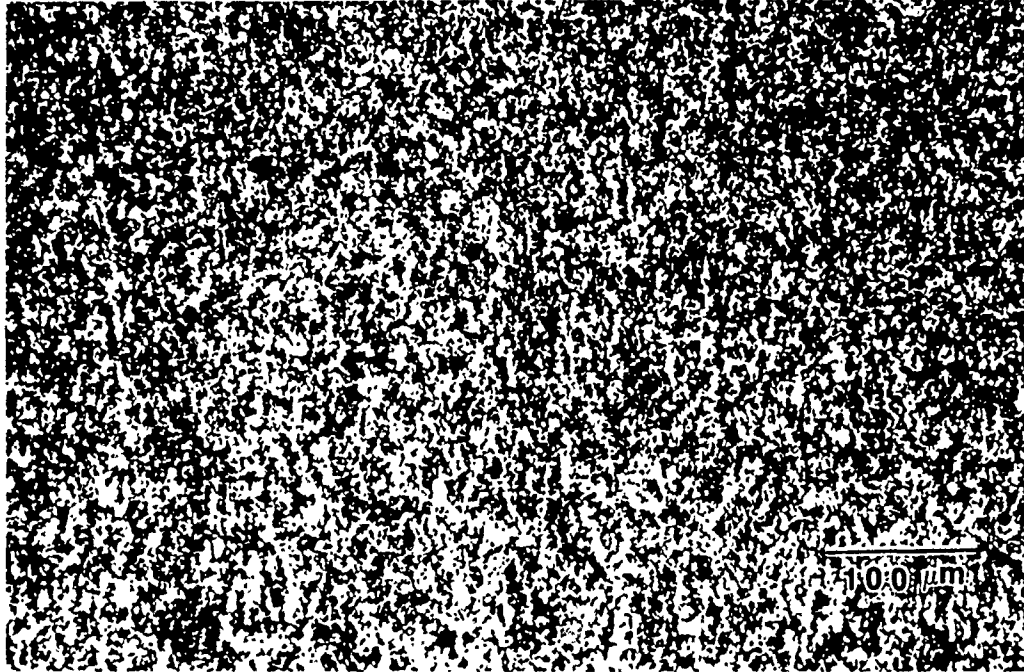


**Figure 17.** View of the Grip Section, Rolled at 150 C and Tested at 370 C and a Strain Rate of  $6.67 \times 10^{-4} \text{ s}^{-1}$ , Depicting Similar Microstructure to the Grip Section in Figure 14 with the Exception of Greater Inclusion Content.



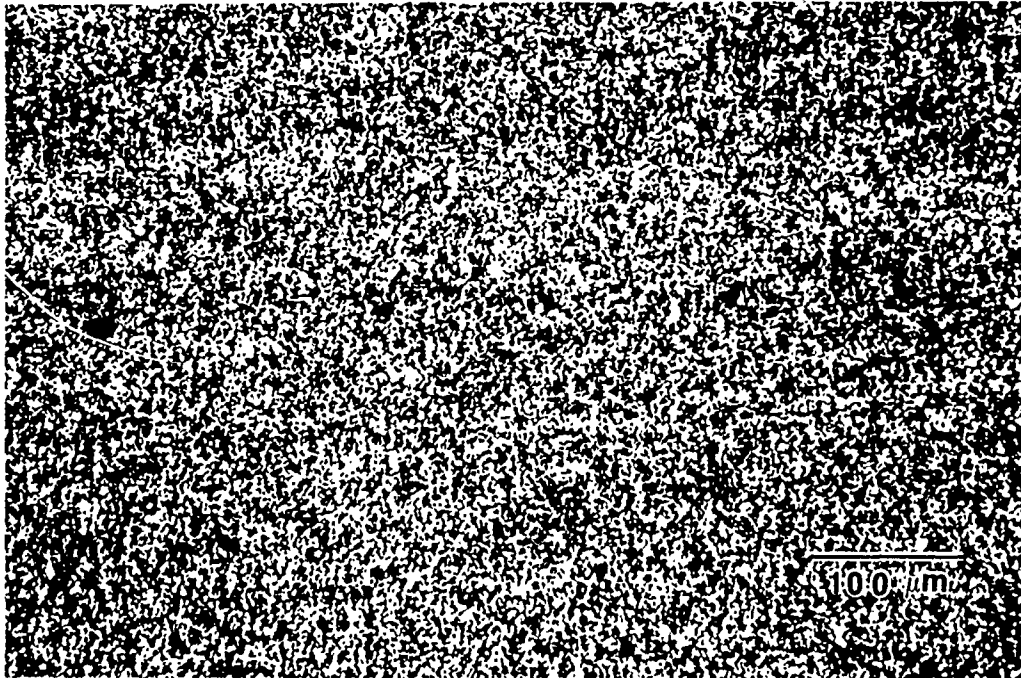


**Figure 18.** Corresponding Gage Section Micrograph to Figure 17, Depicting Retention of Fine Grain Structure, and an Inclusion Content Greater than that Shown in Figures 14 and 15, Possibly Contributing to Failure at an Elongation of only 308%.

along with a historical summary of results from similar previous efforts at NPS, in Appendix 1.

The ultimate objective of a successful TMP is produce  $n$  values close to 0.5. Moderate superplasticity is expected of material exhibiting a coefficient of 0.3. Previous work at NPS failed to yield  $n$  values in even the moderate (0.3) range. Results of the most recent refinements to TMP indicate that this moderate range has now been realized, and this observation is supported by the elongation results reported.

#### **F. SUMMARY**

The low temperature superplasticity model has provided the basis for understanding the TMP employed in this work. Alteration of the TMP, based on this understanding, has resulted in improvement in the degree of CRX achieved. The result has been the progressive enhancement of ductilities obtained during superplastic straining of the Al-2090 alloy.

## V. CONCLUSIONS

The following conclusions may be drawn from this study:

(a) Increasing the amount of strain introduced in the final rolling pass resulted in improved superplastic response.

(b) A refined microstructure was obtained as a result of TMP in each rolling scheme. TEM study will be required to determine the extent of grain boundary misorientation introduced into the material microstructure. While moderate improvement in the materials ductility was obtained, it is apparent that boundary misorientations have not been greatly increased.

(c) Reducing rolling temperature by only 50 C did not result in improved performance.

(d) Reducing rolling temperature to 150 C resulted in improved ductilities at a strain rate of  $6.67 \times 10^{-3} \text{ s}^{-1}$  over a broad temperature range, and produced the maximum elongation realized, (374%) in the study.

(e) The microstructure observed in samples exhibiting the greatest ductility were free of gross formations of porosity.

(f) Strain rate coefficients on the order of 0.3 are observed in material as a result of refinement to TMP.

## VI. RECOMMENDATIONS

The following recommendations are made for continued research in study of superplastic response in 2090 Aluminum:

(a) Investigate the influence of annealing at temperatures in the range of 370-380 C. This represents the same relative percentage of the intermetallic solvi temperature (300 C in Al-Mg alloys) for the  $T_1$  and  $T_2$  phases in Al-2090.

(b) Conduct extensive TEM studies of the evolving microstructure during each step of the TMP. This work should center on the questions of sub-grain formation and grain boundary misalignment at both the completion of each rolling pass and after the subsequent anneal.

## APPENDIX A

### SUMMARY OF ELONGATION DATA

Processing Condition		Elongation (Per Cent)					
Rolling Temp. (C)	Strain Rate (s <sup>-1</sup> )	Test Temperature (C)					
		300	350	370	400	450	500
300	6.67x10 <sup>-2</sup>	43	56	88	76	96	72
300	6.67x10 <sup>-3</sup>	91	102	315	300	326	82
300	6.67x10 <sup>-4</sup>	112	146	175	228	316	48
300	6.67x10 <sup>-5</sup>	165	128	170	143	46	28
250	6.67x10 <sup>-2</sup>		53	84	66	150	
250	6.67x10 <sup>-3</sup>		113	234	226	286	66
250	6.67x10 <sup>-4</sup>		120	212	222	192	
250	6.67x10 <sup>-5</sup>		114	128	146	113	
150	6.67x10 <sup>-2</sup>		88	114	108	136	
150	6.67x10 <sup>-3</sup>		238	328	374	268	
150	6.67x10 <sup>-4</sup>		282	308	240	306	
150	6.67x10 <sup>-5</sup>		222	166	116	178	

Figure A-1. Summary of Ductility Data.

# COMPARISON OF STRAIN RATE SENSITIVITY COEFFICIENTS

TEMP (C)	[Ref. 3] (12-87)  300 C ROLLING	[Ref. 16] (6-88)  350 C ROLLING	[Ref. 4] (3-89)  300 C ROLLING	CURRENT WORK (6-89)		
				ROLLING TEMPERATURE		
				300	250	150
300	0.210			0.306		
350		0.288	0.191	0.263	0.263	0.284
370				0.245	0.249	0.286
400		0.234	0.211	0.310	0.237	0.267
450		0.110		0.323	0.234	0.307
500			0.106	0.047		

Figure A-2. Historical Summary of Strain Rate Sensitivity Coefficients.

## APPENDIX B

### TRUE STRESS VS. TRUE STRAIN

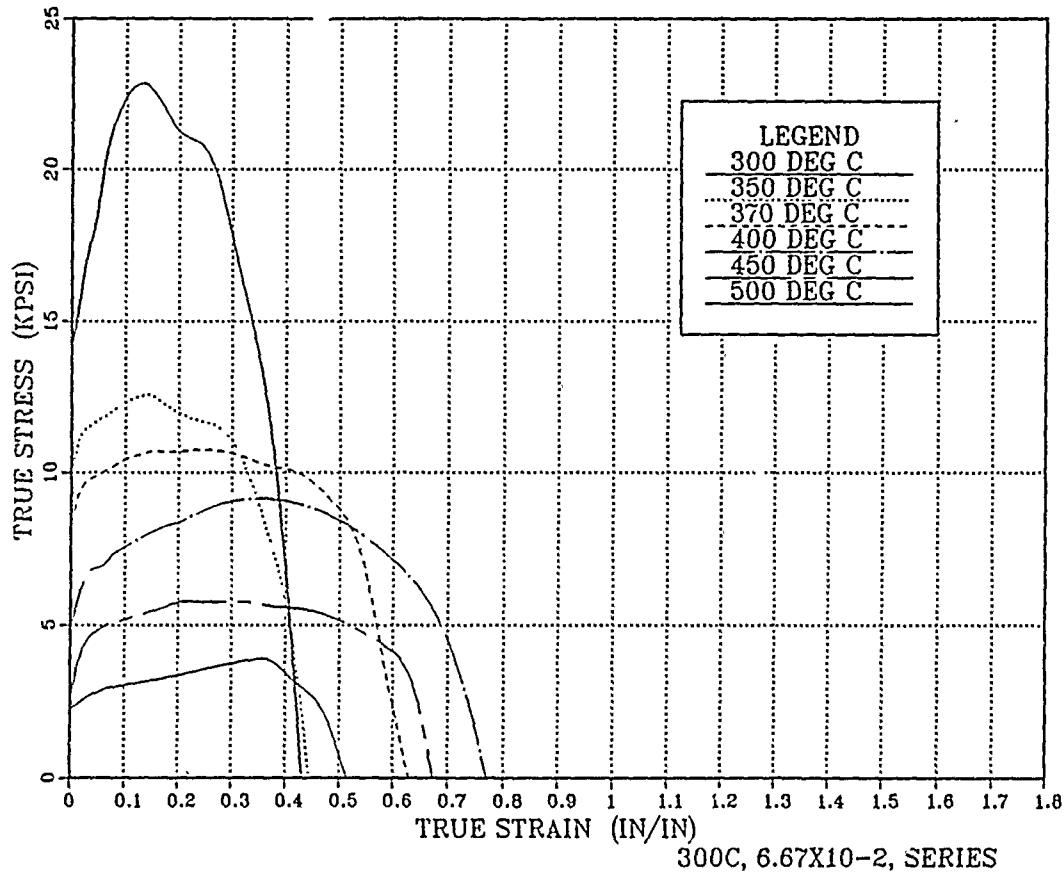


**Figure B-1.** True Stress vs. True Strain for Various Temperatures as Shown in the Legend. The Material was Rolled at a Temperature of 300 C, and Tested at a Strain Rate of  $6.67 \times 10^{-2} \text{ s}^{-1}$ .

## TRUE STRESS VS. TRUE STRAIN

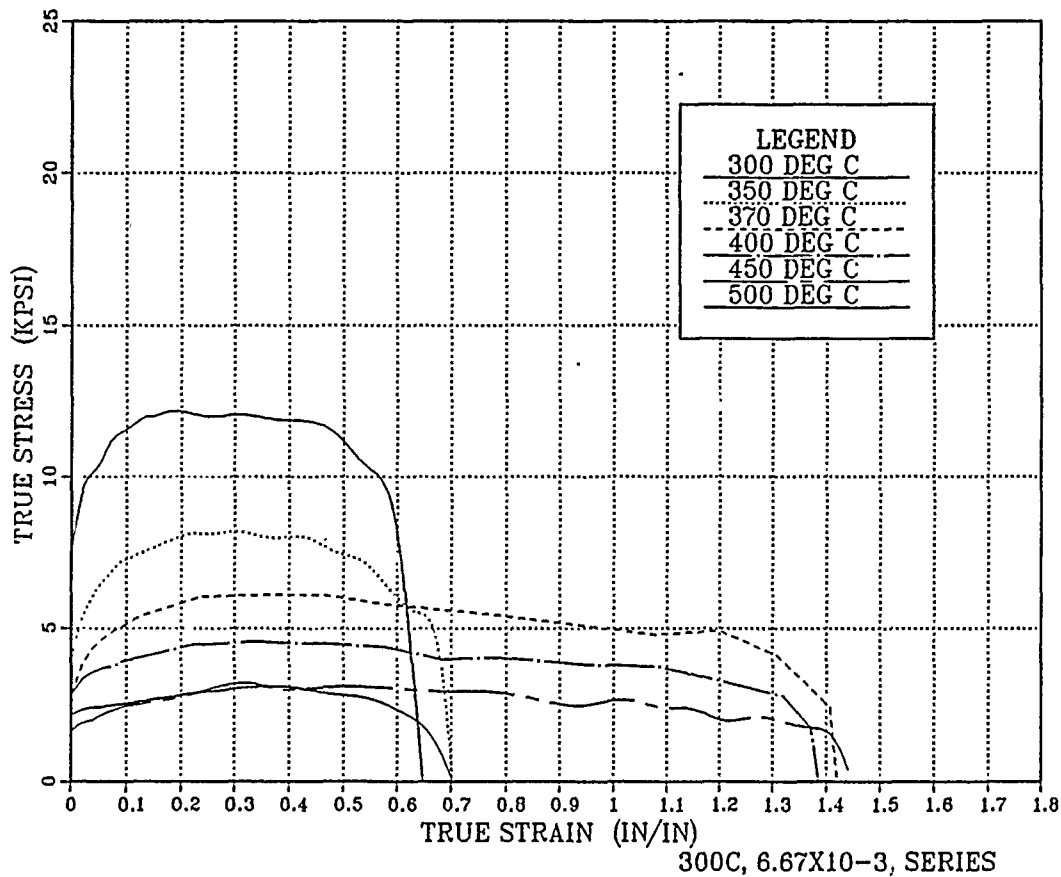


**Figure B-2.** True Stress vs. True Strain for Various Temperatures as Shown in the Legend. The Material was Rolled at a Temperature of 300 C, and Tested at a Strain Rate of  $6.67 \times 10^{-3} \text{ s}^{-1}$ .



## TRUE STRESS VS. TRUE STRAIN

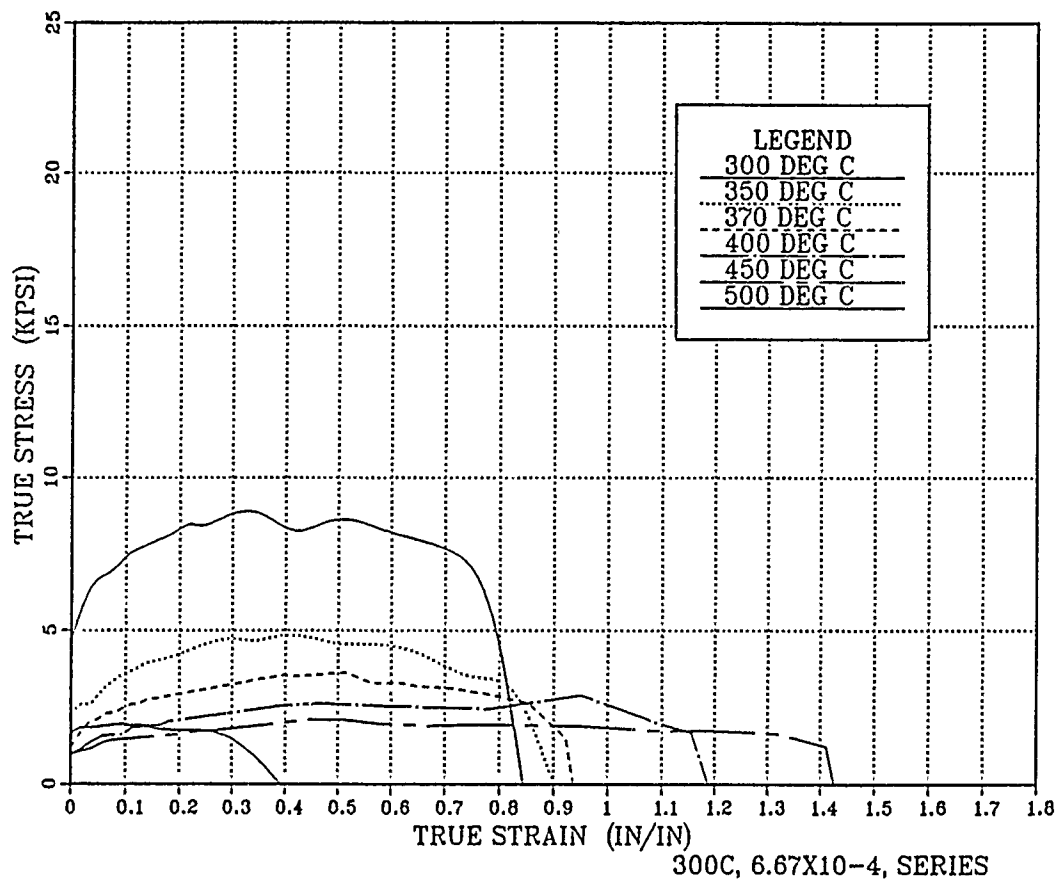


**Figure B-3.** True Stress vs. True Strain for Various Temperatures as Shown in the Legend. The Material was Rolled at a Temperature of 300 C, and Tested at a Strain Rate of  $6.67 \times 10^{-4} \text{ s}^{-1}$ .

## TRUE STRESS VS. TRUE STRAIN

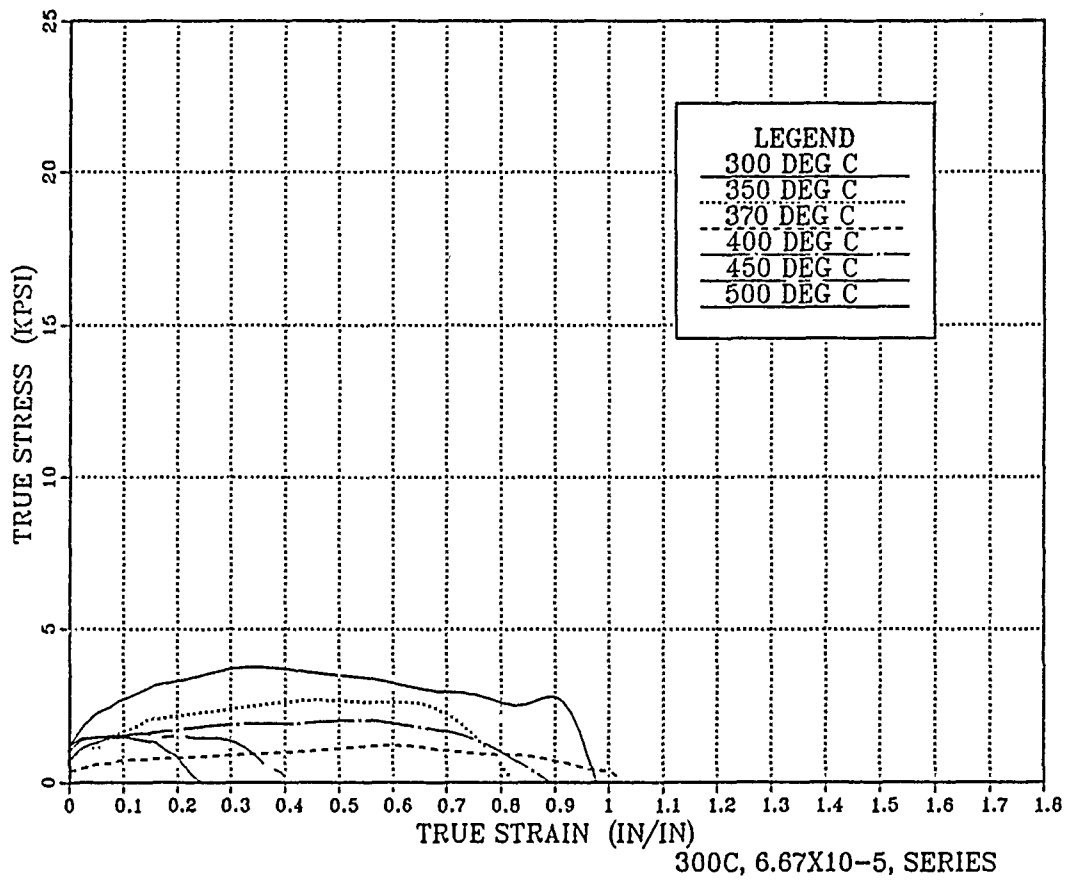


**Figure B-4.** True Stress vs. True Strain for Various Temperatures as Shown in the Legend. The Material was Rolled at a Temperature of 300 C, and Tested at a Strain Rate of  $6.67 \times 10^{-5} \text{ s}^{-1}$ .

## TRUE STRESS VS. TRUE STRAIN

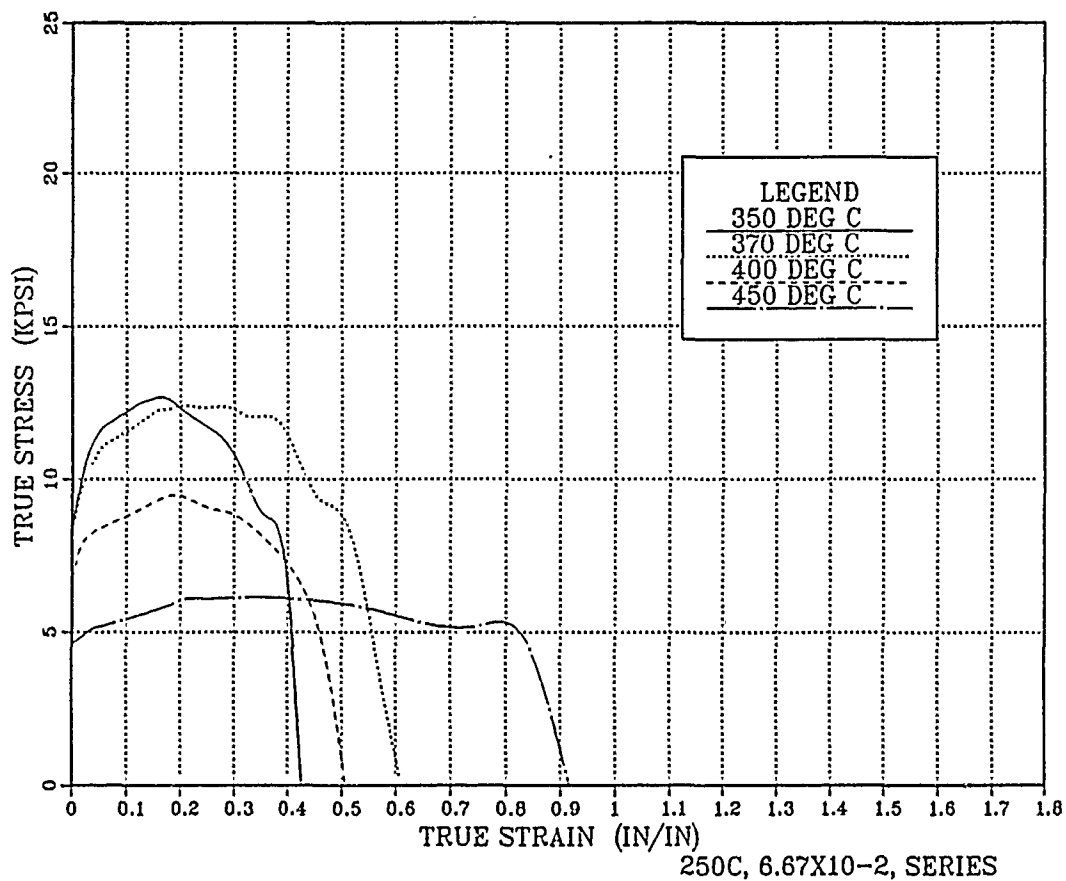


**Figure B-5.** True Stress vs. True Strain for Various Temperatures as Shown in the Legend. The Material was Rolled at a Temperature of 250 C for the Final Five Passes, and Tested at a Strain Rate of  $6.67 \times 10^{-2} \text{ s}^{-1}$ .

## TRUE STRESS VS. TRUE STRAIN

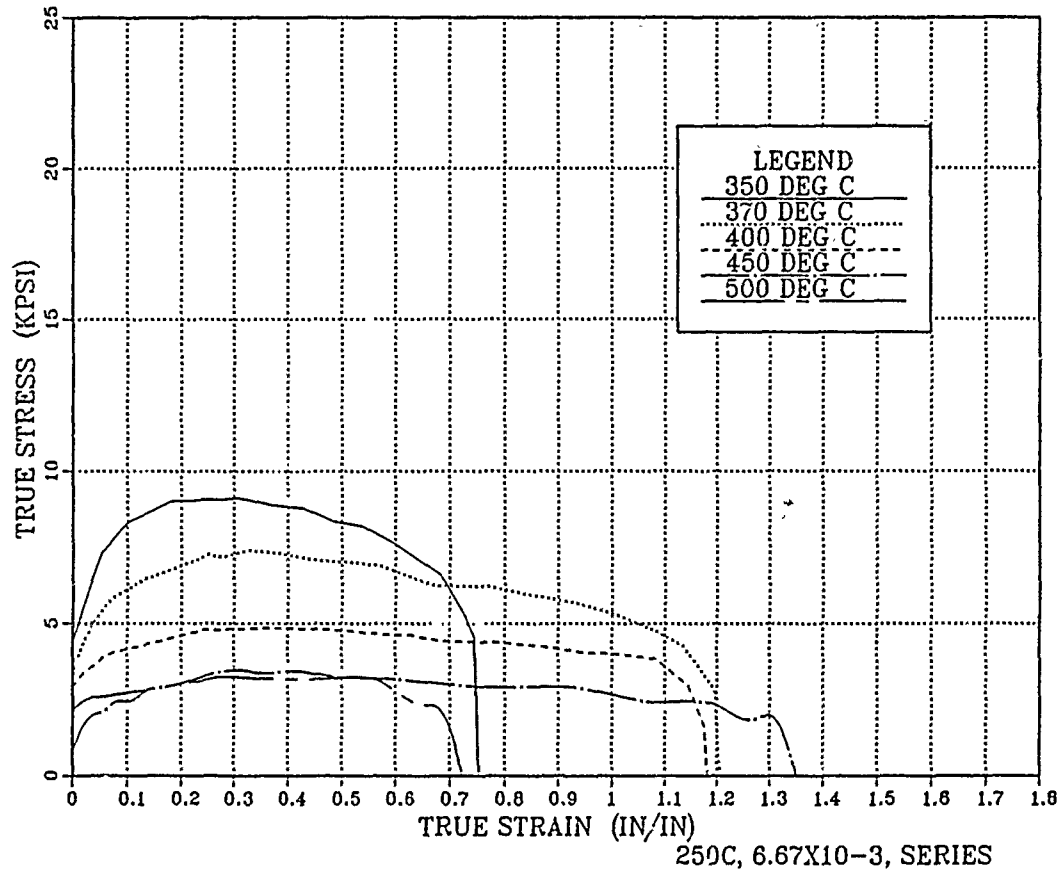


**Figure B-6.** True Stress vs. True Strain for Various Temperatures as Shown in the Legend. The Material was Rolled at a Temperature of 250 C for the Final Five Passes, and Tested at a Strain Rate of  $6.67 \times 10^{-3} \text{ s}^{-1}$ .

## TRUE STRESS VS. TRUE STRAIN

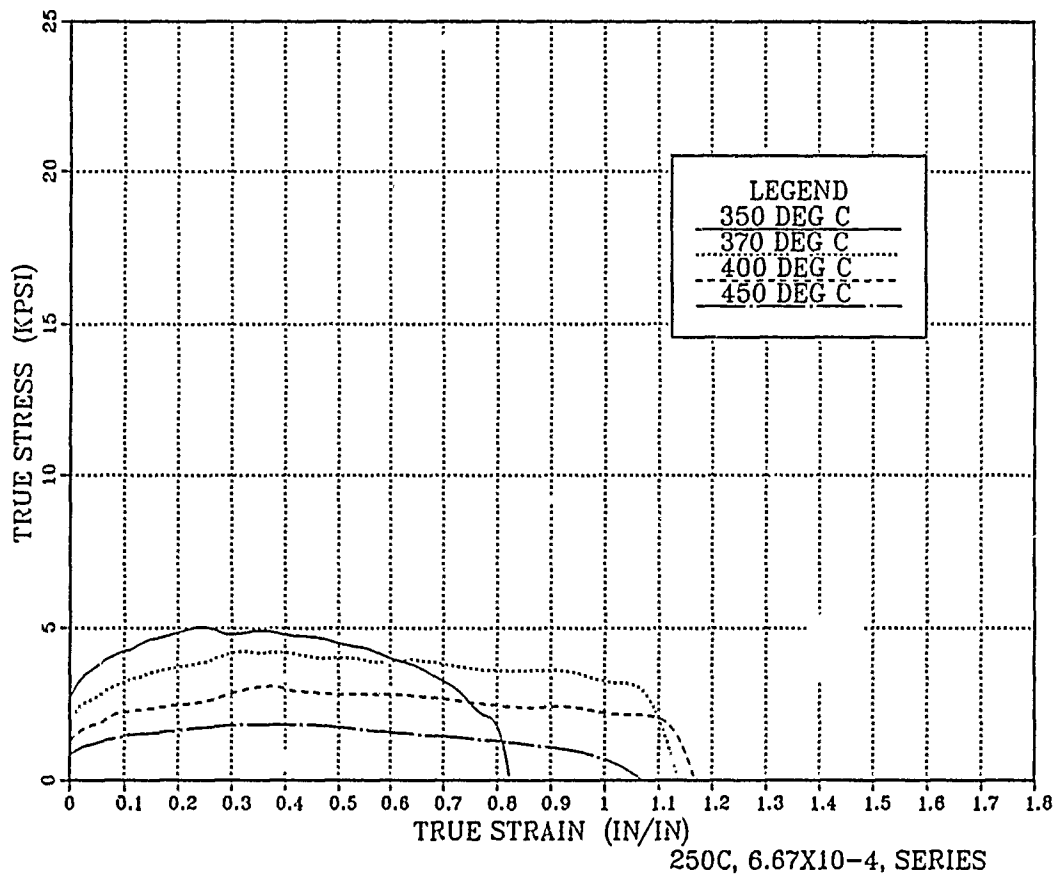


**Figure B-7.** True Stress vs. True Strain for Various Temperatures as Shown in the Legend. The Material was Rolled at a Temperature of 250 C for the Final Five Passes, and Tested at a Strain Rate of  $6.67 \times 10^{-4} \text{ s}^{-1}$ .

## TRUE STRESS VS. TRUE STRAIN

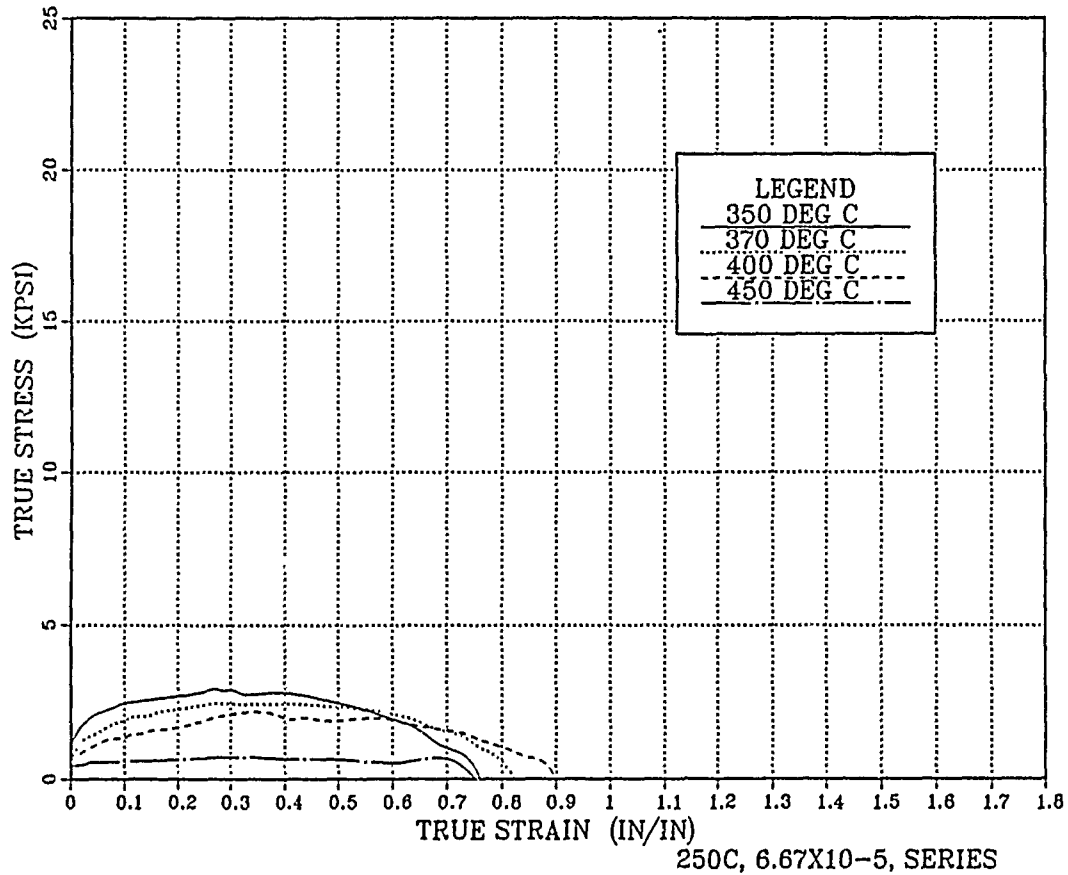


**Figure B-8.** True Stress vs. True Strain for Various Temperatures as Shown in the Legend. The Material was Rolled at a Temperature of 250 C for the Final Five Passes, and Tested at a Strain Rate of  $6.67 \times 10^{-5} \text{ s}^{-1}$ .

# TRUE STRESS VS. TRUE STRAIN

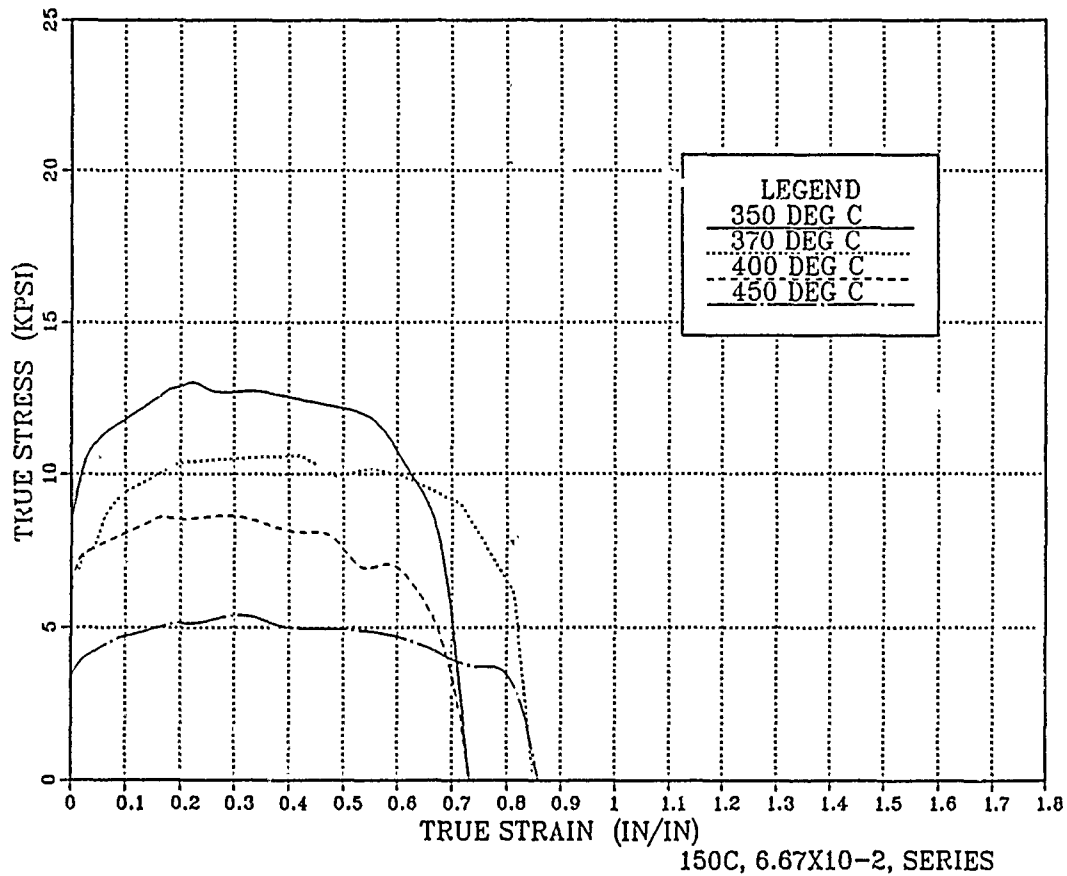


**Figure B-9.** True Stress vs. True Strain for Various Temperatures as Shown in the Legend. The Material was Rolled at a Temperature of 150 C for the Final Five Passes, and Tested at a Strain Rate of  $6.67 \times 10^{-2} \text{ s}^{-1}$ .

## TRUE STRESS VS. TRUE STRAIN

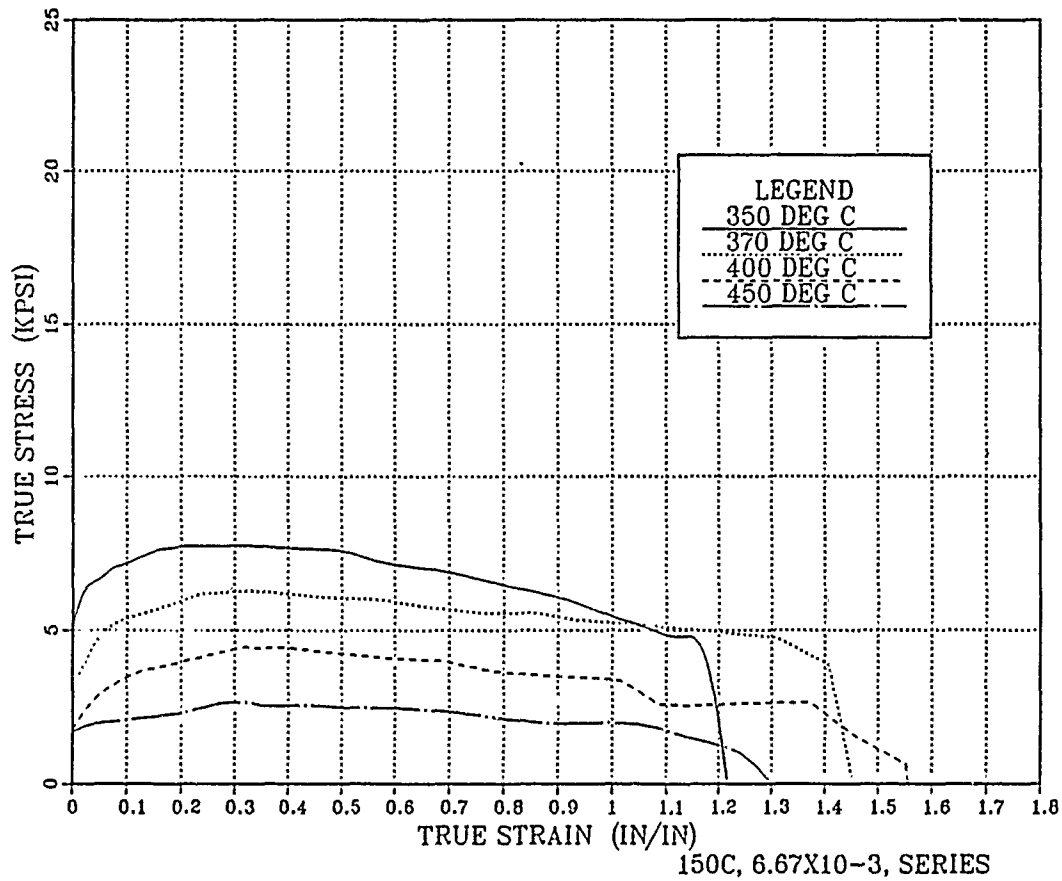


**Figure B-10.** True Stress vs. True Strain for Various Temperatures as Shown in the Legend. The Material was Rolled at a Temperature of 150 C for the Final Five Passes, and Tested at a Strain Rate of  $6.67 \times 10^{-3} \text{ s}^{-1}$ .



# TRUE STRESS VS. TRUE STRAIN

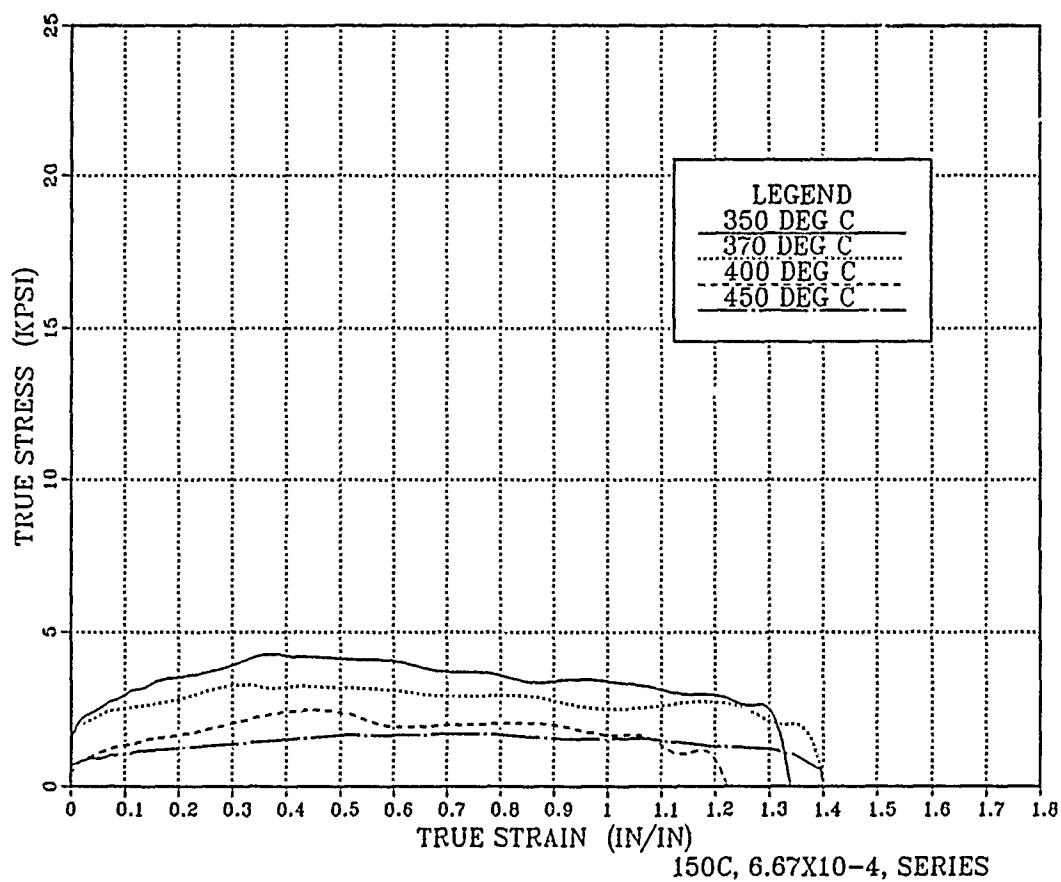


**Figure B-11.** True Stress vs. True Strain for Various Temperatures as Shown in the Legend. The Material was Rolled at a Temperature of 150 C for the Final Five Passes, and Tested at a Strain Rate of  $6.67 \times 10^{-4} \text{ s}^{-1}$ .

## TRUE STRESS VS. TRUE STRAIN

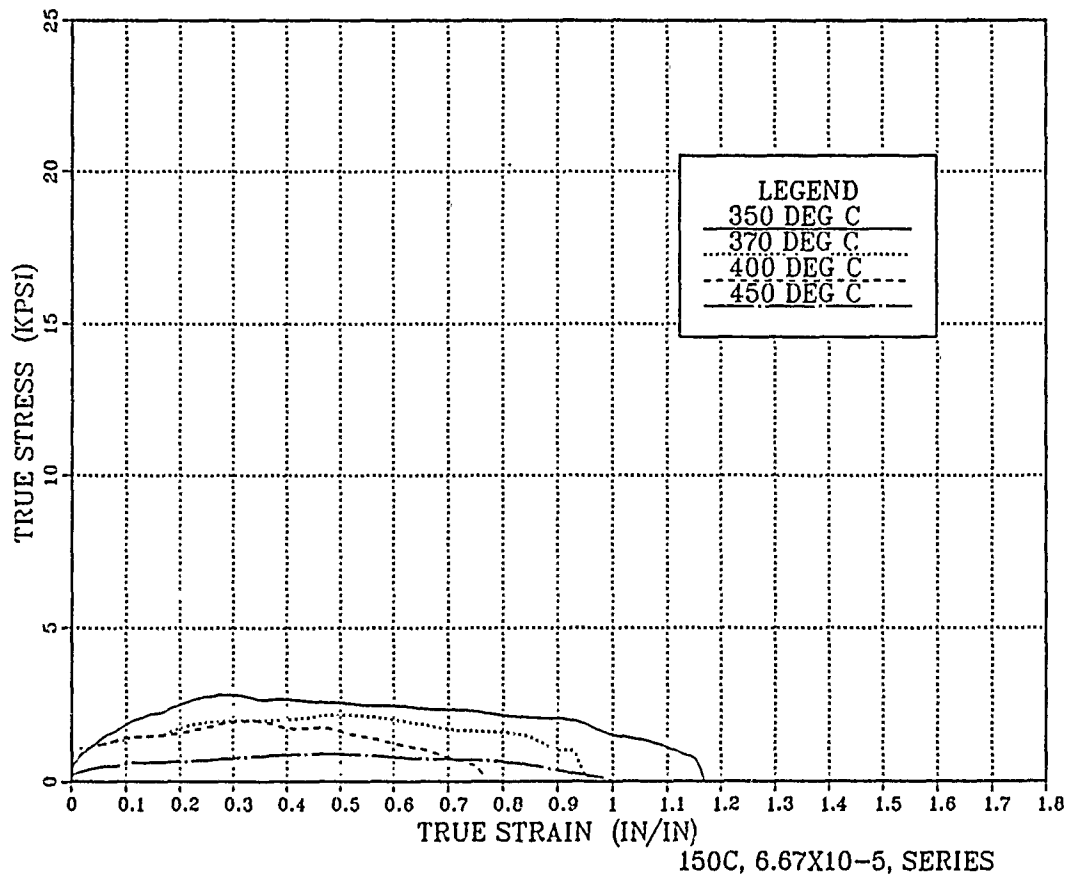


**Figure B-12.** True Stress vs. True Strain for Various Temperatures as Shown in the Legend. The Material was Rolled at a Temperature of 150 C for the Final Five Passes, and Tested at a Strain Rate of  $6.67 \times 10^{-5} \text{ s}^{-1}$ .

# LOG STRESS VS. LOG STRAIN RATE

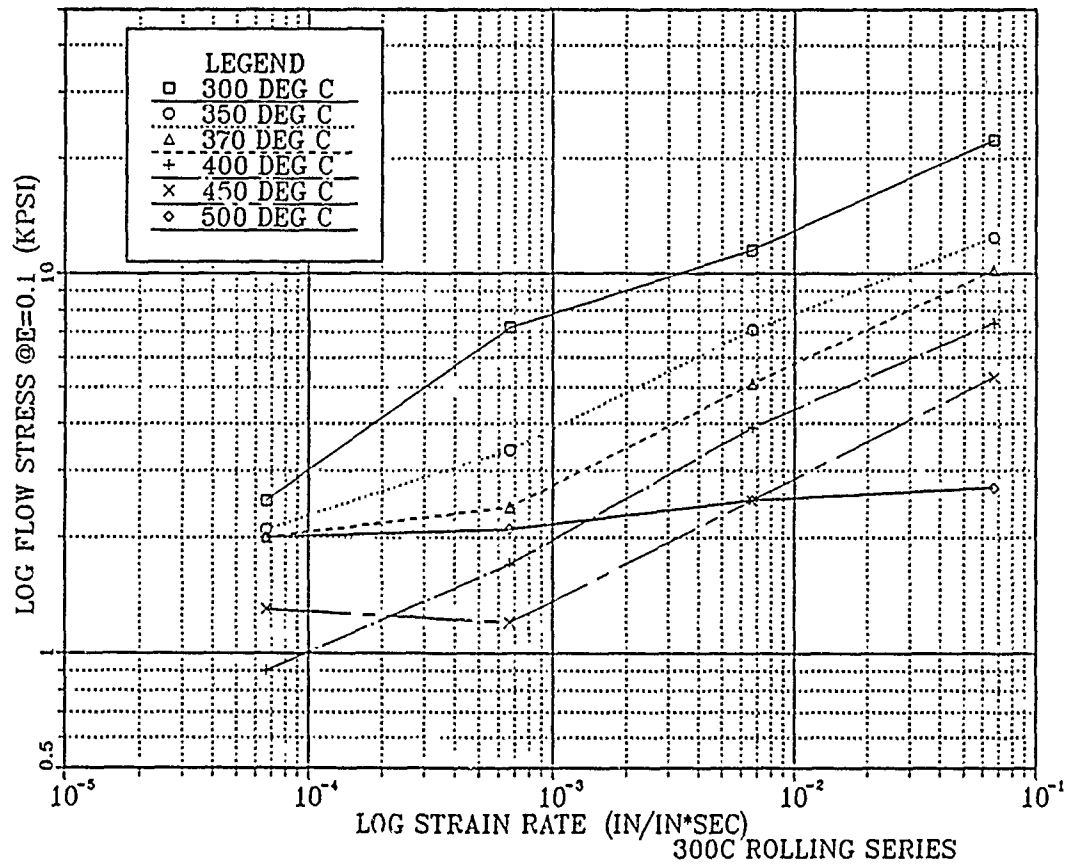


**Figure B-13.** Log Stress vs. Log Strain Rate at a True Strain of 10%, for Various Test Temperatures as Listed in the Legend. For Material Rolled at 300 C.

# LOG STRESS VS. LOG STRAIN RATE

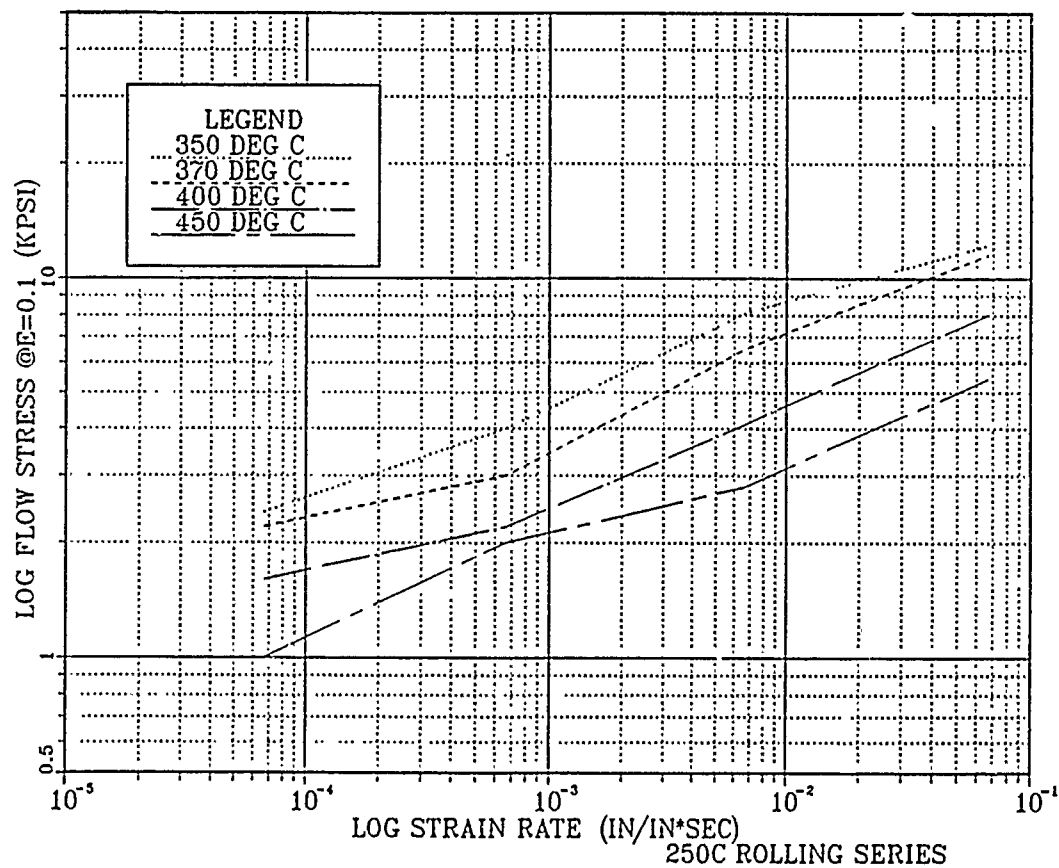


**Figure B-14.** Log Stress vs. Log Strain Rate at a True Strain of 10%, for Various Test Temperatures as Listed in the Legend. For Material Rolled at 250 C in the Final Five Passes.

# LOG STRESS VS. LOG STRAIN RATE

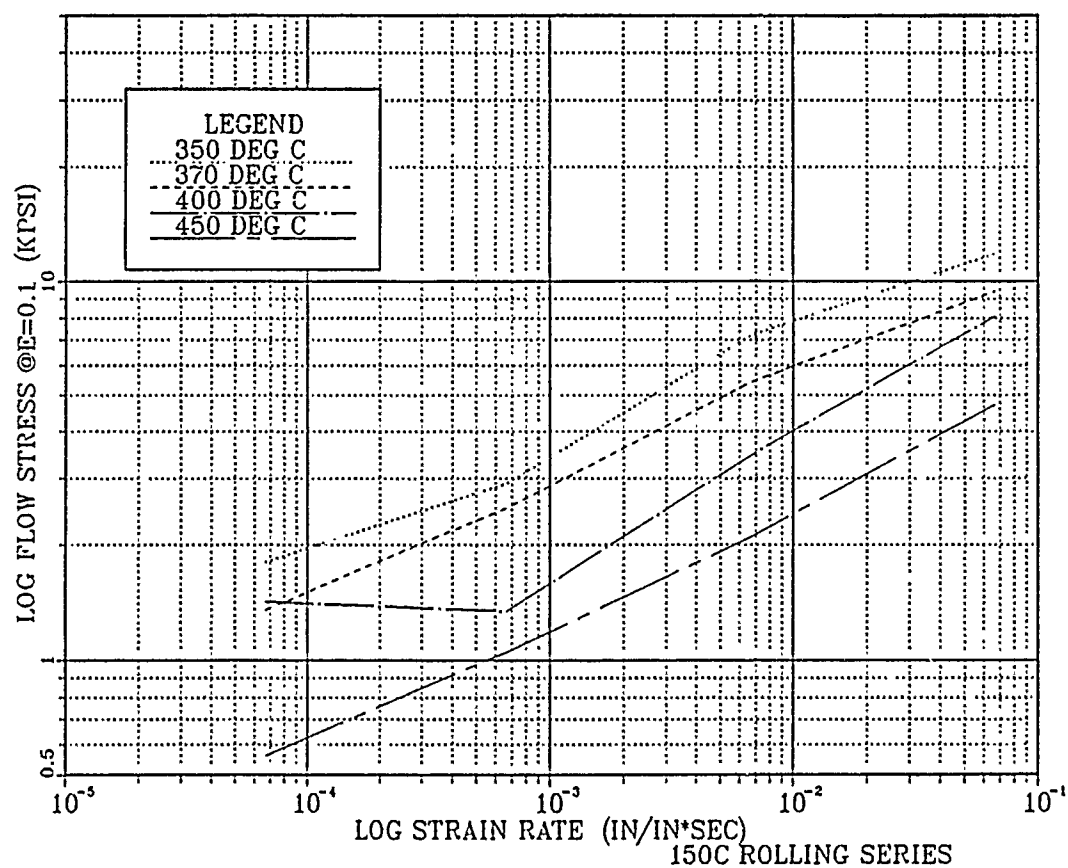


**Figure B-15.** Log Stress vs. Log Strain Rate at a True Strain of 10%, for Various Test Temperatures as Listed in the Legend. For Material Rolled at 150 C in the Final Five Passes.

1. Salama, A. A., Analysis of Grain Refinement and Superplasticity in Aluminum-Magnesium Alloys, Doctoral Dissertation, Naval Postgraduate School, Monterey, California, December 1987.
2. McNelley, T. R., Hales, S. J., and Salama, A. A., "The Mg-Concentration Dependence of the Strength of Al-Mg Alloys During Glide-Controlled Deformation", Scripta Metallurgica, In Print
3. Spiropoulos, P. T., Thermomechanical processing of Al Alloy 2090 for Grain Refinement and Superplasticity, Master's Thesis, Naval Postgraduate School, Monterey, California, December 1987.
4. Choudhry, Mohammad B., Thermomechanical Processing of Aluminum Alloy 2090 for Superplasticity, Master's Thesis, Naval Postgraduate School, Monterey, California, March 1989.
5. Cho, C. W., et al, "Superplasticity of 2090 SPF Sheet at Hot Rolled Gauge", Journal De Physique, C3, pp. 277-283, September 1987.
6. Bampton, C. C., et al, "Superplastic Forming of Aluminum-Lithium Alloy 2090-OE16", Alcoa Laboratories, Alcoa Center, PA 15069.
7. Grimes, R., Miller, W. S., and Butler, R. G., "Development of Superplastic 8090 and 8091 Sheet", Journal De Physic, Collection C3., pp. 239-249, September 1987.
8. Wadsworth, J., Nieh, T. G., and Muklerjee, A. K., "Superplastic Aluminum Alloys-A Review", Aluminum Alloys: Their Physical and Mechanical Properties, Volume II, edited by Starke, E. A. Jr., and Sanders, T. H. Jr., PP. 1239-1246, papers presented at the International Conference, held at the University of Virginia, Charlottesville, Virginia, June 1986.
9. Sherby, O. D., and Wadsworth, J., "Development and Characterization of Fine-Grain Superplastic Materials", Deformation Processing and Structure, edited by Krauss, G., pp. 355-389, American Society for Metals, 1984.
10. Lee, E. W., and McNelley, T. R., "Microstructure Evolution during Processing and Superplastic Flow in a High Magnesium Al-Mg Alloy", Materials Science and Engineering, V. 93, pp. 46-46, 1987.
11. Wadsworth, J., Palmer, I. G., Crooks, D. D., and Lewis, R. E., "Superplastic Behavior of Aluminum-Lithium Alloys", Aluminum-Lithium Alloys, V. II, edited by Sanders, T. H. Jr., and Starke, E. A., pp. 111-137, Proceeding of the Second International Al-Li Conference,

Sponsored by the Non-Ferrous Metal Committee of the Metallurgical Society of AIME, at Monterey, California, 12-14 April 1983.

12. Hales, S. J., and McNelley, T. R., "Microstructural Evolution by Continuous Recrystallization in a Superplastic Al-Mg Alloy", Acta Metallurgica, V. 36, No. 5, pp. 1229-1239, 1988.

13. Dieter, G., Mechanical Metallurgy, pp. 297-300, McGraw-Hill, 1976.

14. Bever, M. B., Massachusetts Institute of Technology, Encyclopedia of Materials Science and Engineering V. 6, pp. 4783-4790, 1986.

15. Encyclopedia of Science and Technology, V. 8, p. 180, McGraw-Hill.

16. Regis, H. C., Processing of 2090 Aluminum Alloy for Superplasticity, Master's Thesis, Naval Postgraduate School, Monterey, California, June 1988.

17. Groh, G. E., Processing of Aluminum Alloy for Superplasticity, Master's Thesis, Naval Postgraduate School, Monterey, California, September 1988.

18. Harris, J. N., Mechanical Working of Metals, pp. \*\*\*, Pergamon Press, New York, 1983.

# INITIAL DISTRIBUTION LIST

		<u>No. Copies</u>
1.	Defense Technical Information Center Cameron Station Alexandria, VA 22304-6145	2
2.	Library, Code 0142 Naval Postgraduate School Monterey, CA 93943-5002	2
3.	Department Chairman, Code 69HY Department of Mechanical Engineering Naval Postgraduate School Monterey, CA 93943-5000	1
4.	Professor T. R. McNelley, Code 69Mc Department of Mechanical Engineering Naval Postgraduate School Monterey, CA 93943-5000	5
5.	Naval Air Systems Command, Code AIR 931 Naval Air Systems Command Headquarters Washington, DC 20361	1
6.	Dr. Eui-Whee Lee, Code 6063 Naval Air Development Center Warminster, PA 18974	1
7.	Dr. Stephen J. Hales Mail Stop 188A NASA-Langley Research Center Hampton, VA 23665-5225	1
8.	Lt. Michael W. Reedy 820 W. Ash St. Piqua, OH 45356	2